Intramolecular feedback regulation of the LRRK2 Roc G domain by a LRRK2 kinase dependent mechanism

Bernd K. Gilsbach[a], Franz Y. Ho[b], Benjamin Riebenbauer[a], Xiaojuan Zhang[b], Giambattista Guaitoli[a], Arjan Kortholt[b,c,*] and Christian Johannes Gloeckner[a,d,*]

[a]German Center for Neurodegenerative diseases (DZNE), Tübingen, Germany

[b]Department of Cell Biochemistry, University of Groningen, Groningen, The Netherlands

[c]YETEM-Innovative Technologies Application and Research Centre Suleyman Demirel University West Campus, Isparta, Turkey

[d]Core Facility for Medical Bioanalytics, Institute for Ophthalmic Research, Center for Ophthalmology, University of Tübingen, Tübingen, Germany

[*]Correspondence:

Arjan Kortholt (a.kortholt@rug.nl)

Christian Johannes Gloeckner (johannes.gloeckner@dzne.de)

Key words: LRRK2, GTPase, kinase, G protein, Michaelis-Menten kinetics, PD, Parkinson's disease, negative feedback loop

Abstract

The Parkinson's Disease (PD)-linked protein Leucine Rich Repeat Kinase 2 (LRRK2) consists of seven domains, including a kinase and a Roc G domain. Despite the availability of several high-resolution structures, the dynamic regulation of its unique intramolecular domain stack is nevertheless still not well understood. By in-depth biochemical analysis, assessing the Michaelis-Menten kinetics of the Roc G domain, we have confirmed that LRRK2 has, similar to other Roco protein family members, a K_M value of LRRK2 that lays within the range of the physiological GTP concentrations within the cell. Furthermore, the R1441G PD variant located within a mutational hotspot in the Roc domain showed an increased catalytic efficiency. In contrast, the most common PD variant G2019S, located in the kinase domain, showed an increased K_M and reduced catalytic efficiency, suggesting a negative feedback mechanism from the kinase domain to the G domain. Autophosphorylation of the G1+2 residue (T1343) in the Roc P-loop motif is critical for this phosphoregulation of both the K_M as well as the k_{cat} values of the Roc-catalyzed GTP hydrolysis, most likely by changing the monomer-dimer equilibrium. The LRRK2 T1343A variant has a similar increased kinase activity in cells compared to G2019S and the double mutant T1343A/G2019S has no further increased activity suggesting that T1343 is crucial for the negative feedback in the LRRK2 signaling cascade. Together our data reveal a novel intramolecular feedback regulation of the LRRK2 Roc G domain by a LRRK2 kinase dependent mechanism. Interestingly, PD mutants differently change the kinetics of the GTPase cycle, which might in part explain the difference in penetrance of these mutations in PD patients.

Introduction

Nonsynonymous sequence variants within the Leucine Rich Repeat Kinase 2 (LRRK2) are associated with familial forms of Parkinson´s disease (PD) and are phenotypically indistinguishable from idiopathic forms of PD (iPD) (Paisan-Ruiz et al., 2004; Zimprich et al., 2004). In addition to defined pathogenic as well as PD-risk coding variants, the LRRK2 locus also contributes to an increased risk of developing iPD more generally, as shown in GWAS studies (Simon-Sanchez et al., 2009). LRRK2 is a multi-domain protein, which belongs to the Roco protein family (Marin et al., 2008). Besides a core module, conserved among the Roco proteins, consisting of a Roc (Ras of complex proteins) G domain and a COR (C-terminal of Roc) dimerization domain, which is followed by a kinase domain, it contains four predicted solenoid domains. The three N-terminal solenoid domains consist of Armadillo repeats followed by an Ankyrin domain and the namesake leucine-rich repeats, while the C-terminus is formed by a seven-bladed WD40 domain (Mills et al., 2012). By similarity, these domains are involved in protein-protein interactions and, based on recent structural models and high-resolution structures, are likely to be involved in the intramolecular regulation of the protein, as well, e.g. by keeping the kinase domain in an auto-inhibited state (Deniston et al., 2020; Gloeckner and Porras, 2020; Guaitoli et al., 2016; Taylor et al., 2020). Moreover, membrane-bound LRRK2 has been demonstrated to phosphorylate a specific set of Rab proteins at a conserved threonine residue within their switch II motif, including Rab8a and Rab10 (Gomez et al., 2019; Steger et al., 2016). In addition, LRRK2 kinase activity has been demonstrated to be involved in endo-lysosomal pathways, thereby being a regulator of the innate immunity (Ahmadi Rastegar and Dzamko, 2020; Bonet-Ponce and Cookson, 2019; Erb and Moore, 2020). Despite these findings, the molecular mechanisms underlying LRRK2 activation and regulation are still not completely understood.

It is clear that the kinase activity of LRRK2 is dependent on the guanine nucleotide binding capacity of the Roc domain. Despite the availability of high-resolution structures, the complete mechanism of G-nucleotide action remains to be determined, in particular if the nucleotide state of the Roc domain influences kinase activity (Biosa et al., 2013; Ito et al., 2007; Taymans et al., 2011).

Previous work on the conserved RocCOR module of a bacterial Roco protein has suggested that the nucleotide state of the Roc domain regulates dimerization (Deyaert et al., 2017). Consistently, also accumulating data shows that a monomer dimer/oligomer transition plays a critical role in LRRK2 protein activation (Berger et al., 2010; Schapansky et al., 2014; Zhu et al., 2023). Cellular data suggest that LRRK2 shuttles between a monomeric cytosolic states and kinase-active oligomeric forms localized at the membrane (Berger et al., 2010; James et al., 2012). Further support comes from recent high-resolution structures, indicating that a Rab29 induced tetramerization represent the kinase active state (Zhu et al., 2023). Our recent data revealed that autophosphorylation induces LRRK2 monomerization

(Guaitoli et al., 2023). Interestingly, the Roc domain has been identified as a major target of LRRK2 autophosphorylation by phospho-proteomic analysis (Gloeckner et al., 2010; Greggio et al., 2009; Webber et al., 2011). Furthermore, there are indications that autophosphorylation of the Roc G domain modifies GTP-binding activities (Webber et al., 2011) and that trans-phosphorylation by the kinase domain of the LRRK2 orthologue *Dictyostelium* Roco4 enhances GTPase activity (Liu et al., 2016). In this study, we analyzed the GTPase activity of LRRK2 and its PD mutants in depth and by combining systematic mutational analysis with the determination of the Michaelis-Menten kinetics. Based on this analysis, we identified an intramolecular negative feedback loop defined by LRRK2 autophosphorylation and its impact on the monomer- dimer equilibrium and GTPase activity.

Results

Impact of PD variants on LRRK2 GTPase activity

We and others have previously determined a full Michaelis-Menten kinetics for the GTPase hydrolysis mediated by Roco proteins as well as for wild-type LRRK2 (Liu et al., 2010; Wauters et al., 2018). LRRK2 has kinetical parameters comparable to other Roco protein family members. Strikingly, the K_M value of LRRK2 lies within the range of the physiological GTP concentrations (around 500 µM (Traut, 1994)) within the cell. Therefore, changes in global cellular or local GTP concentration might have a high impact on protein activity. For this reason, we here fully assessed the enzyme kinetics of disease-associated PD variants, in particular those with confirmed disease co-segregation. For this purpose, we selected three pathogenic variants, R1441G, localized within the Roc domain, the Y1699C variant in the COR-A domain as well as the kinase-domain variant G2019S. All three variants significantly increase the phosphorylation of the LRRK2 substrates Rab8a, Rab10 and Rab12 (Kalogeropulou et al., 2022). In addition to full-length LRRK2 expressed in HEK293T cells, we included a LRRK2 RocCOR domain construct expressed as an MBP fusion protein from *E. coli* in this study. Besides the wild-type, the variants R1441G and Y1699C have been successfully expressed and purified from *E. coli*. For full-length LRRK2, only the Roc-domain variant R1441G as well as the kinase-domain variant G2019S could be analyzed due to considerable low expression and stability of a full-length LRRK2 Y1699C construct in HEK293T cells. LRRK2 wt, R1441G as well as Y1699C MBP-RocCOR constructs showed similar kinetical parameters in the standard radiolabeling assay (charcoal assay), which determines the release of free inorganic phosphate (Pi) (Leupold et al., 1983). While slight differences were observed in the individual K_M as well as k_{cat} values, the catalytic efficiency determined by k_{cat}/K_M was identical (Fig. 1 A-D; Supplemental Table 1). For full-length LRRK2, we have chosen an HPLC-based assay to overcome limitations in the amount of protein necessary to determine a full Michaelis-Menten kinetics. This assay determines the production of GDP by chromatographic separation of the nucleotides (Ahmadian et al., 1997). To ensure that both assays result in comparable results, we compared GTP hydrolysis

rates (k_{obs}) of full-length LRRK2 wt in both assays at two different GTP concentrations. Both assays, the HPLC-based assay as well as the charcoal assay, resulted in overall comparable kinetics, ensuring that the results of both assays can be directly compared (Fig 1E-F; Table 1). For the wild-type full-length LRRK2 protein, we have determined a k_{cat} of 0.36 ± 0.02 min^{-1} and a K_M of 554 ± 62 µM confirming our previously published data thus demonstrating the robustness of the used HPLC-based assay (Wauters et al., 2018).

Interestingly, full-length LRRK2 bearing the R1441G variant, showed a decreased Michaelis-Menten constant (K_M = 271 ± 27 µM) while the k_{cat} increased compared to the wt (Figure 2A) leading to an augmented catalytic efficiency of that variant. In contrast, full-length G2019S LRRK2 showed a significantly increased K_M value of 867 ± 110 µM compared to a wt reference (554 ± 62 µM), while no significant change in the k_{cat} parameter (k_{cat} = 0.36 min^{-1}) was observed (Figure 2B). Together, our data show that LRRK2 has a K_M value that lies within the range of the physiological GTP concentrations and full-length G2019S LRRK2 showed a significantly increased K_M value.

Autophosphorylation regulates GTPase activity

Since the pathogenic G2019S variant has increased kinase activity, we next tested if a kinase-inactive variant has the opposite effect on GTPase activity. In fact, the K_M value (K_M = 181 ± 58 µM) for a K1906M kinase-dead LRRK2 variant is approximately three times lower compared to wt LRRK2 while the k_{cat} value was only slightly reduced (Figure 2C). Consistently, MLi-2 treated fl. wt LRRK2 also has a lower K_M value, which also ensures that the GTPase and not the kinase domain is the driver of the GTP consumption in our experimental set up (Liu and West, 2017). This strongly suggests a negative feedback signal on the Roc domain conferred by an active kinase conformation, most likely mediated via autophosphorylation. To further test this hypothesis, we incubated wild-type LRRK2 with ATP, *in vitro*. In fact, an incubation of the full-length wild-type protein with ATP for two hours at 30°C prior to determining its GTPase activity leads to altered Michaelis-Menten parameters, impacting the K_M as well as k_{cat} values. An approx. twofold increase in K_M (1036 ± 168 µM) and an approx. twofold decrease in k_{cat} (0.13 ± 0.01min^{-1}) demonstrate a strong reduction in LRRK2 GTPase activity by enforced autophosphorylation (Figure 3A). As a control condition, to rule-out inactivation of the LRRK2 protein by degradation during pre-incubation, we incubated a dead variant (K1906M) with ATP, the same way as the wild-type, resulting in no significant change in K_M and k_{cat} values. This shows that autophosphorylation indeed negatively regulates the GTPase activity of LRRK2.

The P-loop site T1343 is a critical site for LRRK2 phosphoregulation

To identify the phospho-sites that are important for the feedback mechanism, we tested several serine/ threonine to alanine mutants (Figure 3B), expecting that the critical autophosphorylation site would show no change in k_{cat} and K_M values for GTP hydrolysis upon *in vitro* ATP treatment. By mass-spectrometric mapping, we and others have previously demonstrated that the Roc domain is a hub for LRRK2 autophosphorylation (Gloeckner et al., 2010; Greggio et al., 2009; Webber et al., 2011).

All Roc autophosphorylation site mutants tested, with the exception of T1343A, showed wild-type behavior upon ATP treatment. A detailed overview of the kinetical analysis of T1343A in comparison to pathogenic variants as well as kinase-dead LRRK2 is shown in Figure 4. In fact, T1343A showed no increase in K_M value after ATP treatment, suggesting that this is the regulatory site which is crucial for the feedback mechanism (Supplemental Figure 2, Figure 3C). In addition to the lower K_M value compared to wild-type that remains unaffected upon ATP treatment, also a reduced k_{cat} value was observed for the T1343A mutant, which might suggest that the mutation is not completely structurally neutral. However, the T1343A mutant does not result in instable or aggregated protein (see below) and, importantly, the T1343A mutant in the RocCOR domain is the only construct that does not significantly affect the GTPase activity (Supplemental-Table 1).

Given that LRRK2 oligomerization is an important mechanism of LRRK2 regulation, at least for LRRK2 kinase activity, we reasoned if the impact of LRRK2 autophosphorylation on the enzymatic properties of the Roc domain is mediated by changes in the oligomeric state of LRRK2. Furthermore, for the Roco protein found in the bacterium *Chlorobium tepidum*, dimerization has been demonstrated to modulate GTPase activity (Deyaert et al., 2017; Gotthardt et al., 2008). In fact, in a recent work we could demonstrate that LRRK2 dimerization is impacted by LRRK2 autophosphorylation (Guaitoli et al., 2023). In this work, we could demonstrate that autophosphorylation is shifting the monomer/dimer (m/d) equilibrium towards the monomeric form. Given the relevance for T1343 phosphorylation on LRRK2 GTPase activity, we wondered, if the observed negative-feedback might be mediated via a modulation of the m/d equilibrium. For this reason, we analyzed the relative abundance of monomers and dimers by mass photometry after ATP treatment for 30 min at 30°C (Guaitoli et al., 2023; Pathak et al., 2023). In contrast to the wild-type, for which the m/d equilibrium could be shifted towards the monomer by *in vitro* autophosphorylation, ATP incubation does not affect the percentage of dimer for the T1343A variant of LRRK2 (Figure 5). This suggests that the underlying mechanism of the negative-feedback phosphorylation towards lower GTPase activity might be mediated by an increased monomerization of LRRK2.

The phospho-null mutant T1343A is sufficient to disrupt the negative feedback in the LRRK2 signaling cascade in cells

Having identified an intramolecular negative-feedback on LRRK2 GTP hydrolysis mediated by autophosphorylation, we were next interested to investigate its relevance in a cellular context. First, we analyzed the kinase activity of T1343A using an *in vitro* LRRKtide assay (Jaleel et al., 2007) to rule out that the unchanged K_M and k_{cat} values observed upon ATP treatment in our GTPase activity assays, are the result of kinase-inactive protein. For this purpose, we compared the kinase activities for LRRK2 T1343A with the wild-type protein, as well as the hyperactive G2019S variant and a kinase-dead control. By this assay, we could clearly demonstrate that T1343A confers specific kinase activity at a level comparable to the LRRK2 wt, while G2019S was clearly more active (Figure 6A). Next, we performed cell-based assays, comparing the phosphorylation levels of the LRRK2 substrate Rab10. To this end, we quantified established markers (pRab10 and pS935) for LRRK2 activity by Western blot analysis (Kalogeropulou et al., 2022) (Figure 6B). In agreement with published data (Kalogeropulou et al., 2022), the other PD mutations R1441G and I2020T showed an approx. 8-fold increase in Rab10 phosphorylation (Figure 6 C-D). Interestingly, the T1343A variant showed an approximately twofold increase in activity which is comparable with G2019S, while the double mutant T1343A/G2019S did not further increase Rab10 phosphorylation (Supplemental Figure 4 and Supplemental Table 3). Together, our results suggest that T1343 is crucial for the negative feedback in the LRRK2 signaling cascade in cells and the mutation to alanine disrupts this regulation. Therefore, the T1343A variant has a similar activity compared to G2019S and the double mutant T1343A/G2019S has no further increased activity.

Discussion

Although there is significant progress toward functional characterization of LRRK2 in the past two decades, including the availability of high-resolution structures covering almost the entire protein in different conformations, the precise molecular mechanisms underlying LRRK2 activation and regulation have yet to be determined (Taymans et al., 2023). One entry point into these mechanisms is based on conserved mechanisms in kinase-associated cellular signaling. Kinases and G-proteins are often found within the same signaling cascade, but with the exception of Roco-proteins, never on the same protein. On the contrary, the usual scheme of signaling is from the G-protein via a kinase cascade towards gene expression is often regulated by the formation of signaling modules orchestrated by scaffolding proteins as given in the well-studied MAP-kinase signaling networks (Birtwistle and Kolch, 2011; Kolch, 2000). In addition, these pathways often include a negative feedback loop allowing a stable signal, a context-specific fine-tuning as well as shut-down of the system (Birtwistle and Kolch, 2011). For example, an EphA2-mediated negative feedback inhibition of the Ras–PI3K–AKT module leads to a cell cycle arrest (Menges and McCance, 2008).

Given that LRRK2 combines a G domain with a kinase domain, resembling canonical signaling modules, besides the investigation of the kinase activity (Taylor et al., 2020), quite some attention has been laid on the analysis of the GTPase activity (Biosa et al., 2013; Ho et al., 2016; Lewis et al., 2007; Liu et al., 2010; Liu et al., 2016; Webber et al., 2011; Wu et al., 2019). Nevertheless, knowledge of the interplay between these two domains is still limited. In addition, observations by most of the studies are based on single k_{obs} values at considerable low GTP concentrations around or below the K_M for full-length LRRK2-mediated GTP hydrolysis and/ or worked with truncated LRRK2 constructs (Liu et al., 2010; Wauters et al., 2018). In this study, we have elucidated a negative feedback loop from kinase to GTPase, increasing the K_M value of the Roc domain via autophosphorylation. Given an average physiological GTP concentration of approx. 500 µM within cells (Traut, 1994), the physiological impact of the differences in the K_M values reported in this study, in combination with a negative feedback loop, is expected to lead to a strong perturbation of the tightly regulated LRRK2 activity. We could observe large changes in the K_M induced by autophosphorylation, which supports our idea of an intramolecular negative-feedback. This feedback loop has an inhibitory effect on LRRK2 Roc-mediated GTP hydrolysis. Furthermore, our study revealed that different PD variants not only alter kinase but also change the kinetics of the Roc-mediated GTP hydrolysis. In fact, when looking at the catalytic efficiency it is striking that we found it to be increased for the R1441G variant located within a mutational hotspot of the Roc domain, also containing the PD variants R1441C, H and S, which is in good agreement with the penetrance of these variants (Haugarvoll et al., 2008). In contrast, the most prevalent LRRK2 PD variant G2019S shows an increase in K_M, while the catalytic efficiency remains unchanged. This finding is also in well agreement with the different impact of these pathogenic variants on the Rab phosphorylation. While R1441G shows a strong Rab phosphorylation in cells, the effect mediated by G2019S is considerably weaker (Kalogeropulou et al., 2022). Furthermore, we could demonstrate that LRRK2 kinase activity is negatively regulating the Roc-mediated GTP hydrolysis.

By a systematic mutational analysis, removing confirmed phospho-sites within the Roc domain, we identified with T1343 a critical residue, involved in the autophosphorylation mediated negative feedback, in contrast to LRRK2 wt it also showed no difference in dimer-monomer formation upon ATP treatment. T1343 has initially been mapped by phosphoproteomic studies (Gloeckner et al., 2010; Greggio et al., 2009). Furthermore, it has been shown to be quantitatively phosphorylated in the C-terminal four-domain 'RCKW' construct allowing resolving the phospho-threonine in the recently published cryo-EM structure (Deniston et al., 2020). T1343A and T1343G variants have already been tested in two previous studies, however only at basal conditions and/or *in vitro* where similar activity was observed in comparison to wild-type LRRK2 (Biosa et al., 2013; Stormer et al., 2023). In agreement with our data, no effect of T1343G on *in vitro* kinase activity was observed (Stormer et al., 2023). Furthermore, replacing T1343 by a non-phosphorylatable residue reduced P^{33} incorporation in

phosphorylation assays by 50% (Greggio et al., 2009). As the new AlphaFold3 deep learning-based modelling software became available, recently, allowing to consider PTMs as well as small molecules, we compared the models of the GDP vs the GTP-state of pT1343 LRRK2 (Abramson et al., 2024). Interestingly, the AF3 model suggests, that the phosphate of the pT1343 is orientated inwards thereby substituting the gamma phosphate (see Supplemental Figure 5). This finding is in well agreement with MD simulations published recently (Stormer et al., 2023). As we are determining GTP hydrolysis in a multi turnover situation, the pT1343 might hamper the hydrolysis by competing with GTP re-binding. Interestingly, according to phosphoproteomes curated in the PhosphoSitePlus database (www.phoshposite.org) also other Rabs are phosphorylated either at a conserved serine or threonine residue at the homologous position (G1+2) within the P-loop (for a P-loop alignment of all Rabs see: (Mishra et al., 2013)), including Rab1a, Rab5a, Rab7a, Rab8a, Rab10, Rab13, Rab15, Rab17 and Rab35 as well as Rab2 and Rab22a, respectively. In addition, also Rab4, Rab34 are phosphorylated at a P-loop residue. Furthermore, the atypical Rab protein Rab24, has a phosphorylatable Tyrosine (Y17) at this position (Ding et al., 2003). In agreement with the findings for LRRK2 described here, Rab24 Y17A shows an increase intrinsic GTP hydrolysis rate (Wu et al., 2006). Together, these findings suggest, that P-loop phosphorylation is a relevant and conserved regulatory mechanism for Rab proteins.

What might be the biological consequence of this mechanism? As shown for its bacterial orthologue (Deyaert et al., 2017), increasing the GTP-loaded portion of LRRK2 favor its monomeric state. GTP hydrolysis leads, at least transiently, to a GDP-bound state of LRRK2, potentially inducing dimerization at a critical local protein concentration. LRRK2 kinase activity might counteract this mechanism by autophosphorylation of the P-loop residue T1343, shifting the equilibrium back to the monomeric state. This hypothesis is supported by recently determined EM structures of the bacterial LRRK2 homologue ctRoco (Galicia et al., 2024). This CtRoco dimer structure revealed a dimer-stabilized orientation of the P-loop, which would prevent direct nucleotide binding on the dimer. This therefore further supports a critical role of the P-loop conformation in the nucleotide-induced monomerization Removing of this regulatory phosphosite leads to an LRRK2 activity comparable to G2019S, and cannot be further increased by introducing the double mutant T1343A/G2019S. This suggests that there is a tight regulation between GTPase activity, phosphorylation and monomer dimer equilibrium which all interplay with each other to regulate the LRRK2 signal output. Consistently, compounds target either the kinase, G domain or dimerization can block LRRK2 activity and signaling (Helton et al., 2021; Pathak et al., 2023; Wojewska and Kortholt, 2021).

However, to fully understand the LRRK2 mechanism and further explore allosteric targeting of LRRK2, a better understanding of the complex and dynamic conformational changes underlying the local orchestration and activation of LRRK2, in particular in the context of membrane localization and

oligomerization as well as effector binding, such as Rab12 and Rab29 or 14-3-3 (reviewed in: (Alessi and Pfeffer, 2024)), is necessary.

In conclusion, our study describes a novel intramolecular feedback mechanism of LRRK2, which is based on autophosphorylation. Similar to MAPK pathways where negative feedback mechanisms are essential to guarantee a robust signal, and also allowing a tight and context-specific shutdown of the pathway, the kinase domain in its active conformation negatively regulates GTP hydrolysis.

Material and Methods

DNA Constructs. Cloning of the LRRK2 cDNA from human lymphoblasts has been described in Gloeckner et al., 2006 (Gloeckner et al., 2006). The LRRK2 cDNA was cloned into pDONR202 vector and further subcloned by the Gateway(TM) LR-reaction (Invitrogen) into the pDEST-NSF-TAP vector for the expression of an N-terminal FLAG/ tandem-STREP tag II tagged fusion protein (Gloeckner et al., 2007). Variants were introduced into the ENTRY construct by site-directed mutagenesis using the QuikChange(TM) II XL kit (Agilent). For the expression of the RocCOR construct in bacteria, a cDNA sequence corresponding to the LRRK2 amino acids 1293-1840 was subcloned into the pDEST-566 vector (N-terminal 6xHIS-MBP tag) using the Gateway(TM) system. pDEST-566 was a gift from Dominic Esposito (Addgene plasmid #11517; http://n2t.net/addgene:11517; RRID: Addgene_11517).

Purification of full-length LRRK2 from HEK293T cells. The purification of NSF-tagged full-length LRRK2 has been performed as described previously with minor adaptations (Guaitoli et al., 2016). Briefly, HEK293T cells (CRL-11268; American Type Culture Collection) were transfected between 50% and 70% confluence with 8 µg of plasmid DNA/ 14 cm culture dish using polyethyleneimine (PEI) 25 kDa (Polysciences), and cultured post-transfection for 48 hrs in 14 cm dishes in DMEM (Sigma-Aldrich) supplemented with 10% (vol/vol) FBS (Sigma-Aldrich) and appropriate antibiotics. After removal of the medium, the cells were resuspended in lysis buffer (1 mL / 14 cm dish) containing 30 mM Tris (pH 8.0), 150 mM NaCl, 5mM $MgCl_2$, 3 mM DTE, 5% Glycerol and supplemented with 0.5 % (v/v) Nonidet P-40 substitute, complete protease inhibitor (Roche) and 0.1 mM GDP. Cell lysis was allowed to proceed for 1 h at 4°C on a rotating shaker (10 rpm) and cell debris and nuclei were removed by centrifugation at 10,000 × g for 10 min. The lysate was incubated with Strep-Tactin beads (IBA, 500 µl bed volume / 15 mL cell lysate) for 2 h at 4°C on a rotating shaker. The beads were transferred to a microspin column (GE healthcare) and washed extensively 5x with washing buffer (30 mM Tris (pH 8.0), 150 mM NaCl, 3 mM DTT, 5 mM $MgCl_2$, 5 % [vol/vol] glycerol) containing 0.1 mM GDP. Elution was performed with 500 µL of the same washing buffer containing 2.5 mM of D-Desthiobiotin (IBA) and 0.1 mM GDP.

Purified proteins were further concentrated using ultracell-30 centrifugal filter units (30 kDa cutoff, Amicon) to reduce relative GDP amounts.

Purification of 6xHIS-MBP-RocCOR from *E. coli*. 6xHIS-MBP-RocCOR was purified according to standard protocols with minor adaptations (Riggs, 2001). Briefly, the RocCOR pDEST-566 vector was transformed in the E. coli BL21(DE3) strain. An overnight culture was used to inoculate into 2 L LB medium and grow at 37°C. When the culture reached an OD at 600 nm of about 0.7, protein expression was induced with 0.6 mM IPTG for 4 h at 20°C. Cells were harvested and resuspended in resuspension buffer (50 mM HEPES pH 8, 150 mM NaCl, 10 mM $MgCl_2$, 10 % Glycerol, 0.5 mM GDP and 5 mM β-mercaptoethanol, supplemented with 1 mM PMSF and 1x cOmplete™ EDTA-free protease inhibitor cocktail (Roche)), and then lysed by sonication. The cell lysate was clarified by centrifugation at 70,000 x g, 4°C for 1 hr. The cleared cell lysate was loaded on a 5 mL MBPTrap column (GE Healthcare). The captured proteins were washed with 5 CV wash buffer (20 mM HEPES pH 8, 200 mM NaCl, 10 mM $MgCl_2$, 10 % Glycerol, 0.5 mM GDP and 5 mM β-mercaptoethanol), then 10 CV wash buffer supplemented with 5 mM ATP, and finally again with 5 CV wash buffer. The MBP fused protein was eluted in wash buffer containing 10 mM maltose.

HPLC-based GTP hydrolysis assay. Steady-state kinetic measurements of LRRK2-mediated GTP hydrolysis were performed as previously described (Ahmadian et al., 1997). Briefly, 0.1 µM of full-length LRRK2 was incubated with different amounts of GTP (0, 25, 75, 150, 250, 500, 1000, 2000, 3000 and 5000 µM) and production of GDP was monitored by reversed phase C18 HPLC. To this end, the samples (10 µl) were directly injected on a reversed-phase C18 column (pre-column: Hypersil Gold, 3µm particle size, 4.6x10mm; main column: Hypersil Gold, 5µm particle size, 4.6x250mm, Thermo Scientific) using an Ultimate 3000 HPLC system (Thermo Scientific, Waltham, MA, USA) in HPLC-buffer containing 50 mM KH_2PO_4/K_2HPO_4 pH 6.0, 10 mM tetrabutylammonium bromide and 10-15% acetonitrile. Subsequently, samples were analyzed using the HPLC integrator (Chromeleon 7.2, Thermo Scientific, Waltham, MA, USA). Initial rates of GDP production were plotted against the GTP concentration using GraFit5 (v.5.0.13, Erithacus Software). The number of experiments is indicated in the graph and data point is the average (±s.e.m.) of indicated repetitions. The Michaelis-Menten equation was fitted to determine K_M (±s.e.) and k_{cat} (±s.e.).

HPLC-based LRRKtide assay. LRRK2, LRRKtide and ATP were mixed on ice to a final concentration 0.1 µM LRRK2, 200 µM LRRKtide and 1 mM ATP, in 30 mM Tris/HCl pH 8.0, 150 mM NaCl, 10 mM $MgCl_2$, 5 mM DTE, 5% Glycerol, 0.1 mM GDP. Samples were taken at 0, 5, 10, 25, 45, 65, 90 and 120 min. To stop the reaction TFA was added to a final concentration of 0.1% and the samples were kept on ice before HPLC analysis. To separate phospho from non-phospho LRRKtide the following HPLC protocol was used: Hypersil Gold C18 (2.1x150 mm; 3 µm particle size, Thermo Scientific), Buffer A: 5% ACN, 0.1

% TFA, Buffer B: 80% ACN, 0.1% TFA, flow rate at 0.5 ml/min, detection at 202nm. The Elution profile was as follows: 0-1 min 100% Buffer A, 1-15 min Gradient up to 60% Buffer B, 15-17 min 100% Buffer B, 17-22 min 100% Buffer A. Subsequently, samples were analyzed using the HPLC integrator (Chromeleon 7.2, Thermo Scientific, Waltham, MA, USA). Rates of phospho-LRRKtide production were plotted against the time using GraFit5 (v.5.0.13, Erithacus Software).

Charcoal GTP hydrolysis assay. The [γ-32P]GTP charcoal assay was performed as previously described (Bollag and McCormick, 1995). Briefly, 0.1 µM full-length LRRK2 or 0.5 µM 6xHIS-MBP-RocCOR was incubated with different GTP concentrations, ranging from 75 µM to 8 mM, in the presence of [γ-^{32}P] GTP in GTPase assay buffer (30 mM Tris pH 8, 150 mM NaCl, 10 mM $MgCl_2$, 5% (v/v) Glycerol and 3 mM DTT). Samples were taken at different time-points and immediately quenched with 5% activated charcoal in 20 mM phosphoric acid. All non-hydrolyzed GTP and proteins were stripped by the activated charcoal and sedimented by centrifugation. The radioactivity of the isolated inorganic phosphates was then measured by scintillation counting. The initial rates of γ-phosphate release and the Michaelis-Menten kinetics were calculated as described above.

Mass photometry. MP was performed as described in (Guaitoli et al., 2023). Briefly, the dimer ratio of LRRK2 was determined on a Refeyn Two MP instrument (Refeyn). Prior to the experiment, a standard curve relating particle contrasts to molecular weight was established using a Native molecular weight standard (Invitrogen, 1:200 dilution in HEPES-based elution buffer: 50 mM HEPES [pH 8.0], 150 mM NaCl supplemented with 200 µM desthiobiotin). The LRRK2 protein was diluted to 2x of the final concentration (end concentration: 75 nM) in elution buffer. The optical setup was focused in 10 µl elution buffer before adding 10 µl of the adjusted protein sample. Depending on the obtained count numbers, acquisition times were chosen between 20 s to 1 min. The dimer ratio in each measurement was normalize according to the equation.

$$Normalized\ dimer\ \% = \frac{Dimer\ \%}{Monomer\ \% + Dimer\ \%}$$

Three measurements were processed for each experimental condition, and data were analyzed by GraphPad Prism.

Cell-based Rab assay. Cell-based LRRK2 activity assays were performed as previously described (Singh et al., 2022). Briefly, HEK293T cells were cultured in DMEM (supplemented with 10% Fetal Bovine Serum and 0.5% Pen/Strep). For the assay, the cells were seeded onto six-well plates and transfected at a confluency of 50-70% with SF-tagged LRRK2 variants using PEI-based lipofection. After 48 hours cells were lysed in lysis buffer [30 mM Tris-HCl (pH7.4), 150 mM NaCl, 1% NonidentP-40 substitute, complete protease inhibitor cocktail, PhosStop phosphatase inhibitors (Roche)]. Lysates were cleared

by centrifugation at 10,000 x g and adjusted to a protein concentration of 1 µg/µl in 1x Laemmli Buffer. Samples were subsequently subjected to SDS PAGE and Western Blot analysis to determine LRRK2 pS935 and Rab10 T73 phosphorylation levels, as described below. Total LRRK2 and Rab10 levels were determined as a reference for normalization. For Western blot analysis, protein samples were separated by SDS–PAGE using NuPAGE 10% Bis-Tris gels (Invitrogen) and transferred onto PVDF membranes (Thermo Fisher). To allow simultaneous probing for LRRK2 on the one hand and Rab10 on the other hand, membranes were cut horizontally at the 140 kDa MW marker band. After blocking non-specific binding sites with 5% non-fat dry milk in TBST (1 h, RT) (25 mM Tris, pH 7.4, 150 mM NaCl, 0.1% Tween-20), membranes were incubated overnight at 4°C with primary antibodies at dilutions specified below. Phospho-specific antibodies were diluted in TBST/ 5% BSA (Roth GmbH). Non-phospho-specific antibodies were diluted in TBST/ 5% non-fat dry milk powder (BioRad). Phospho-Rab10 levels were determined by the site-specific rabbit monoclonal antibody anti-pRAB10(pT73) (Abcam, ab230261) and LRRK2 pS935 was determined by the site-specific rabbit monoclonal antibody UDD2 (Abcam, ab133450), both at a dilution of 1:2,000. Total LRRK2 levels were determined by the in-house rat monoclonal antibody anti-pan-LRRK2 (clone 24D8; 1:10,000) (Carrion et al., 2017). Total Rab10 levels were determined by the rabbit monoclonal antibody anti-RAB10/ERP13424 (Abcam, ab181367) at a dilution of 1:5,000. For detection, goat anti-rat IgG or anti-rabbit IgG HRP-coupled secondary antibodies (Jackson ImmunoResearch) were used at a dilution of 1:15,000 in TBST/ 5% non-fat dry milk powder. Antibody–antigen complexes were visualized using the ECL plus chemiluminescence detection system (GE Healthcare) using the Stella imaging system (Raytest) for detection and quantification.

Data analysis. GTP hydrolysis was determined from metadata extracted from the chromatograms. Based on these data, Michaelis-Menten fits were performed using GraFit5 (v5.0.13). Statistical significance of reported differences between the conditions was determined by ANOVA using Tukey post hoc test.

Data availability

Raw data for Western blot quantifications are shown in the supplement. AlphaFold3 models have been generated under AlphaFold Server Output Terms of Use on the AlphaFold server (www.alphafoldserver.com, date: 05/09/2024). Final models have been deposited on Zenodo (https://doi.org/10.5281/zenodo.11242230).

Author contributions

B.K.G., F.Y.H. and B.R. performed LRRK2 GTPase and kinase activity assays. G.G and X.Z. performed the mass photometry measurements. A.K. and C.J.G. designed the study. B.K.G., F.Y.H., A.K. and C.J.G. wrote the manuscript.

Acknowledgements

The authors are grateful to Felix von Zweydorf as well as to the working students for their technical assistance in cloning the different LRRK2 variants and maintaining the plasmids.

Funding

The work was supported by The Michael J. Fox Foundation for Parkinson's Research (grant No: 8068.04 to C.J.G. and A.K.).

References

Abramson, J., Adler, J., Dunger, J., Evans, R., Green, T., Pritzel, A., Ronneberger, O., Willmore, L., Ballard, A.J., Bambrick, J., Bodenstein, S.W., Evans, D.A., Hung, C.C., O'Neill, M., Reiman, D., Tunyasuvunakool, K., Wu, Z., Zemgulyte, A., Arvaniti, E., Beattie, C., Bertolli, O., Bridgland, A., Cherepanov, A., Congreve, M.*, et al.* (2024). Accurate structure prediction of biomolecular interactions with AlphaFold 3. *Nature* doi: 10.1038/s41586-024-07487-w.

Ahmadi Rastegar, D., and Dzamko, N. (2020). Leucine Rich Repeat Kinase 2 and Innate Immunity. *Front Neurosci 14*, 193 doi: 10.3389/fnins.2020.00193.

Ahmadian, M.R., Hoffmann, U., Goody, R.S., and Wittinghofer, A. (1997). Individual rate constants for the interaction of Ras proteins with GTPase-activating proteins determined by fluorescence spectroscopy. *Biochemistry 36*, 4535-4541 doi: 10.1021/bi962556y.

Alessi, D.R., and Pfeffer, S.R. (2024). Leucine-Rich Repeat Kinases. *Annual review of biochemistry* doi: 10.1146/annurev-biochem-030122-051144.

Berger, Z., Smith, K.A., and Lavoie, M.J. (2010). Membrane localization of LRRK2 is associated with increased formation of the highly active LRRK2 dimer and changes in its phosphorylation. *Biochemistry 49*, 5511-5523 doi: 10.1021/bi100157u.

Biosa, A., Trancikova, A., Civiero, L., Glauser, L., Bubacco, L., Greggio, E., and Moore, D.J. (2013). GTPase activity regulates kinase activity and cellular phenotypes of Parkinson's disease-associated LRRK2. *Human molecular genetics 22*, 1140-1156 doi: 10.1093/hmg/dds522.

Birtwistle, M.R., and Kolch, W. (2011). Biology using engineering tools: the negative feedback amplifier. *Cell Cycle 10*, 2069-2076 doi: 10.4161/cc.10.13.16245.

Bollag, G., and McCormick, F. (1995). Intrinsic and GTPase-activating protein-stimulated Ras GTPase assays. *Methods in enzymology 255*, 161-170 doi: 10.1016/s0076-6879(95)55020-8.

Bonet-Ponce, L., and Cookson, M.R. (2019). The role of Rab GTPases in the pathobiology of Parkinson' disease. *Curr Opin Cell Biol 59*, 73-80 doi: 10.1016/j.ceb.2019.03.009.

Carrion, M.D.P., Marsicano, S., Daniele, F., Marte, A., Pischedda, F., Di Cairano, E., Piovesana, E., von Zweydorf, F., Kremmer, E., Gloeckner, C.J., Onofri, F., Perego, C., and Piccoli, G. (2017). The LRRK2 G2385R variant is a partial loss-of-function mutation that affects synaptic vesicle trafficking through altered protein interactions. *Sci Rep 7*, 5377 doi: 10.1038/s41598-017-05760-9.

Deniston, C.K., Salogiannis, J., Mathea, S., Snead, D.M., Lahiri, I., Matyszewski, M., Donosa, O., Watanabe, R., Bohning, J., Shiau, A.K., Knapp, S., Villa, E., Reck-Peterson, S.L., and Leschziner, A.E. (2020). Structure of LRRK2 in Parkinson's disease and model for microtubule interaction. *Nature 588*, 344-349 doi: 10.1038/s41586-020-2673-2.

Deyaert, E., Wauters, L., Guaitoli, G., Konijnenberg, A., Leemans, M., Terheyden, S., Petrovic, A., Gallardo, R., Nederveen-Schippers, L.M., Athanasopoulos, P.S., Pots, H., Van Haastert, P.J.M., Sobott, F., Gloeckner, C.J., Efremov, R., Kortholt, A., and Versees, W. (2017). A homologue of the Parkinson's disease-associated protein LRRK2 undergoes a monomer-dimer transition during GTP turnover. *Nature communications 8*, 1008 doi: 10.1038/s41467-017-01103-4.

Ding, J., Soule, G., Overmeyer, J.H., and Maltese, W.A. (2003). Tyrosine phosphorylation of the Rab24 GTPase in cultured mammalian cells. *Biochemical and biophysical research communications 312*, 670-675 doi: 10.1016/j.bbrc.2003.10.171.

Erb, M.L., and Moore, D.J. (2020). LRRK2 and the Endolysosomal System in Parkinson's Disease. *J Parkinsons Dis 10*, 1271-1291 doi: 10.3233/JPD-202138.

Galicia, C., Guaitoli, G., Fislage, M., Gloeckner, C.J., and Versées, W. (2024). Structural insights in the GTP-driven monomerization and activation of a bacterial LRRK2 homologue using allosteric nanobodies. *eLife 13*, RP94503 doi: 10.7554/eLife.94503.

Gloeckner, C.J., Boldt, K., Schumacher, A., Roepman, R., and Ueffing, M. (2007). A novel tandem affinity purification strategy for the efficient isolation and characterisation of native protein complexes. *Proteomics 7*, 4228-4234 doi: 10.1002/pmic.200700038.

Gloeckner, C.J., Boldt, K., von Zweydorf, F., Helm, S., Wiesent, L., Sarioglu, H., and Ueffing, M. (2010). Phosphopeptide analysis reveals two discrete clusters of phosphorylation in the N-terminus and the Roc domain of the Parkinson-disease associated protein kinase LRRK2. *Journal of proteome research 9*, 1738-1745 doi: 10.1021/pr9008578.

Gloeckner, C.J., Kinkl, N., Schumacher, A., Braun, R.J., O'Neill, E., Meitinger, T., Kolch, W., Prokisch, H., and Ueffing, M. (2006). The Parkinson disease causing LRRK2 mutation I2020T is associated with increased kinase activity. *Human molecular genetics 15*, 223-232 doi: 10.1093/hmg/ddi439.

Gloeckner, C.J., and Porras, P. (2020). Guilt-by-Association - Functional Insights Gained From Studying the LRRK2 Interactome. *Front Neurosci 14*, 485 doi: 10.3389/fnins.2020.00485.

Gomez, R.C., Wawro, P., Lis, P., Alessi, D.R., and Pfeffer, S.R. (2019). Membrane association but not identity is required for LRRK2 activation and phosphorylation of Rab GTPases. *J Cell Biol 218*, 4157-4170 doi: 10.1083/jcb.201902184.

Gotthardt, K., Weyand, M., Kortholt, A., Van Haastert, P.J., and Wittinghofer, A. (2008). Structure of the Roc-COR domain tandem of C. tepidum, a prokaryotic homologue of the human LRRK2 Parkinson kinase. *The EMBO journal 27*, 2239-2249 doi: 10.1038/emboj.2008.150.

Greggio, E., Taymans, J.M., Zhen, E.Y., Ryder, J., Vancraenenbroeck, R., Beilina, A., Sun, P., Deng, J., Jaffe, H., Baekelandt, V., Merchant, K., and Cookson, M.R. (2009). The Parkinson's disease kinase LRRK2 autophosphorylates its GTPase domain at multiple sites. *Biochemical and biophysical research communications 389*, 449-454 doi: 10.1016/j.bbrc.2009.08.163.

Guaitoli, G., Raimondi, F., Gilsbach, B.K., Gomez-Llorente, Y., Deyaert, E., Renzi, F., Li, X., Schaffner, A., Jagtap, P.K., Boldt, K., von Zweydorf, F., Gotthardt, K., Lorimer, D.D., Yue, Z., Burgin, A., Janjic, N., Sattler, M., Versees, W., Ueffing, M., Ubarretxena-Belandia, I., Kortholt, A., and Gloeckner, C.J. (2016). Structural model of the dimeric Parkinson's protein LRRK2 reveals a compact architecture involving distant interdomain contacts. *Proceedings of the National Academy of Sciences of the United States of America 113*, E4357-4366 doi: 10.1073/pnas.1523708113.

Guaitoli, G., Zhang, X., Saitta, F., Miglionico, P., Silbermann, L.M., Ho, F.Y., Zweydorf, F.v., Signorelli, M., Tych, K., Fessas, D., Raimondi, F., Kortholt, A., and Gloeckner, C.J. (2023). Biophysical analysis reveals autophosphorylation as an important negative regulator of LRRK2 dimerization. Preprint available at *bioRxiv*, 2023.2008.2011.549911 doi: 10.1101/2023.08.11.549911.

Haugarvoll, K., Rademakers, R., Kachergus, J.M., Nuytemans, K., Ross, O.A., Gibson, J.M., Tan, E.K., Gaig, C., Tolosa, E., Goldwurm, S., Guidi, M., Riboldazzi, G., Brown, L., Walter, U., Benecke, R., Berg, D., Gasser, T., Theuns, J., Pals, P., Cras, P., De Deyn, P.P., Engelborghs, S., Pickut, B., Uitti, R.J.*, et al.* (2008). Lrrk2 R1441C parkinsonism is clinically similar to sporadic Parkinson disease. *Neurology 70*, 1456-1460 doi: 10.1212/01.wnl.0000304044.22253.03.

Helton, L.G., Soliman, A., von Zweydorf, F., Kentros, M., Manschwetus, J.T., Hall, S., Gilsbach, B., Ho, F.Y., Athanasopoulos, P.S., Singh, R.K., LeClair, T.J., Versees, W., Raimondi, F., Herberg, F.W.,

Gloeckner, C.J., Rideout, H., Kortholt, A., and Kennedy, E.J. (2021). Allosteric Inhibition of Parkinson's-Linked LRRK2 by Constrained Peptides. *ACS chemical biology 16*, 2326-2338 doi: 10.1021/acschembio.1c00487.

Ho, D.H., Jang, J., Joe, E.H., Son, I., Seo, H., and Seol, W. (2016). G2385R and I2020T Mutations Increase LRRK2 GTPase Activity. *Biomed Res Int 2016*, 7917128 doi: 10.1155/2016/7917128.

Ito, G., Okai, T., Fujino, G., Takeda, K., Ichijo, H., Katada, T., and Iwatsubo, T. (2007). GTP binding is essential to the protein kinase activity of LRRK2, a causative gene product for familial Parkinson's disease. *Biochemistry 46*, 1380-1388 doi: 10.1021/bi061960m.

Jaleel, M., Nichols, R.J., Deak, M., Campbell, D.G., Gillardon, F., Knebel, A., and Alessi, D.R. (2007). LRRK2 phosphorylates moesin at threonine-558: characterization of how Parkinson's disease mutants affect kinase activity. *The Biochemical journal 405*, 307-317 doi: 10.1042/BJ20070209.

James, N.G., Digman, M.A., Gratton, E., Barylko, B., Ding, X., Albanesi, J.P., Goldberg, M.S., and Jameson, D.M. (2012). Number and brightness analysis of LRRK2 oligomerization in live cells. *Biophys J 102*, L41-43 doi: 10.1016/j.bpj.2012.04.046.

Kalogeropulou, A.F., Purlyte, E., Tonelli, F., Lange, S.M., Wightman, M., Prescott, A.R., Padmanabhan, S., Sammler, E., and Alessi, D.R. (2022). Impact of 100 LRRK2 variants linked to Parkinson's Disease on kinase activity and microtubule binding. *The Biochemical journal* doi: 10.1042/BCJ20220161.

Kolch, W. (2000). Meaningful relationships: the regulation of the Ras/Raf/MEK/ERK pathway by protein interactions. *The Biochemical journal 351 Pt 2*, 289-305 doi:

Leupold, C.M., Goody, R.S., and Wittinghofer, A. (1983). Stereochemistry of the elongation factor Tu X GTP complex. *Eur J Biochem 135*, 237-241 doi: 10.1111/j.1432-1033.1983.tb07643.x.

Lewis, P.A., Greggio, E., Beilina, A., Jain, S., Baker, A., and Cookson, M.R. (2007). The R1441C mutation of LRRK2 disrupts GTP hydrolysis. *Biochemical and biophysical research communications 357*, 668-671 doi: 10.1016/j.bbrc.2007.04.006.

Liu, M., Dobson, B., Glicksman, M.A., Yue, Z., and Stein, R.L. (2010). Kinetic mechanistic studies of wild-type leucine-rich repeat kinase 2: characterization of the kinase and GTPase activities. *Biochemistry 49*, 2008-2017 doi: 10.1021/bi901851y.

Liu, Z., Mobley, J.A., DeLucas, L.J., Kahn, R.A., and West, A.B. (2016). LRRK2 autophosphorylation enhances its GTPase activity. *FASEB journal : official publication of the Federation of American Societies for Experimental Biology 30*, 336-347 doi: 10.1096/fj.15-277095.

Liu, Z., and West, A.B. (2017). The dual enzyme LRRK2 hydrolyzes GTP in both its GTPase and kinase domains in vitro. *Biochim Biophys Acta Proteins Proteom 1865*, 274-280 doi: 10.1016/j.bbapap.2016.12.001.

Marin, I., van Egmond, W.N., and van Haastert, P.J. (2008). The Roco protein family: a functional perspective. *FASEB journal : official publication of the Federation of American Societies for Experimental Biology 22*, 3103-3110 doi: 10.1096/fj.08-111310.

Menges, C.W., and McCance, D.J. (2008). Constitutive activation of the Raf-MAPK pathway causes negative feedback inhibition of Ras-PI3K-AKT and cellular arrest through the EphA2 receptor. *Oncogene 27*, 2934-2940 doi: 10.1038/sj.onc.1210957.

Mills, R.D., Mulhern, T.D., Cheng, H.C., and Culvenor, J.G. (2012). Analysis of LRRK2 accessory repeat domains: prediction of repeat length, number and sites of Parkinson's disease mutations. *Biochemical Society transactions 40*, 1086-1089 doi: 10.1042/BST20120088.

Mishra, A.K., Del Campo, C.M., Collins, R.E., Roy, C.R., and Lambright, D.G. (2013). The Legionella pneumophila GTPase activating protein LepB accelerates Rab1 deactivation by a non-canonical hydrolytic mechanism. *The Journal of biological chemistry 288*, 24000-24011 doi: 10.1074/jbc.M113.470625.

Myasnikov, A., Zhu, H., Hixson, P., Xie, B., Yu, K., Pitre, A., Peng, J., and Sun, J. (2021). Structural analysis of the full-length human LRRK2. *Cell 184*, 3519-3527 e3510 doi: 10.1016/j.cell.2021.05.004.

Paisan-Ruiz, C., Jain, S., Evans, E.W., Gilks, W.P., Simon, J., van der Brug, M., Lopez de Munain, A., Aparicio, S., Gil, A.M., Khan, N., Johnson, J., Martinez, J.R., Nicholl, D., Marti Carrera, I., Pena, A.S., de Silva, R., Lees, A., Marti-Masso, J.F., Perez-Tur, J., Wood, N.W., and Singleton, A.B.

(2004). Cloning of the gene containing mutations that cause PARK8-linked Parkinson's disease. *Neuron 44*, 595-600 doi: 10.1016/j.neuron.2004.10.023.

Pathak, P., Alexander, K.K., Helton, L.G., Kentros, M., LeClair, T.J., Zhang, X., Ho, F.Y., Moore, T.T., Hall, S., Guaitoli, G., Gloeckner, C.J., Kortholt, A., Rideout, H., and Kennedy, E.J. (2023). Doubly Constrained C-terminal of Roc (COR) Domain-Derived Peptides Inhibit Leucine-Rich Repeat Kinase 2 (LRRK2) Dimerization. *ACS Chem Neurosci 14*, 1971-1980 doi: 10.1021/acschemneuro.3c00259.

Riggs, P. (2001). Expression and purification of maltose-binding protein fusions. *Curr Protoc Mol Biol Chapter 16*, Unit16 16 doi: 10.1002/0471142727.mb1606s28.

Schapansky, J., Nardozzi, J.D., Felizia, F., and LaVoie, M.J. (2014). Membrane recruitment of endogenous LRRK2 precedes its potent regulation of autophagy. *Human molecular genetics 23*, 4201-4214 doi: 10.1093/hmg/ddu138.

Simon-Sanchez, J., Schulte, C., Bras, J.M., Sharma, M., Gibbs, J.R., Berg, D., Paisan-Ruiz, C., Lichtner, P., Scholz, S.W., Hernandez, D.G., Kruger, R., Federoff, M., Klein, C., Goate, A., Perlmutter, J., Bonin, M., Nalls, M.A., Illig, T., Gieger, C., Houlden, H., Steffens, M., Okun, M.S., Racette, B.A., Cookson, M.R*., et al.* (2009). Genome-wide association study reveals genetic risk underlying Parkinson's disease. *Nat Genet 41*, 1308-1312 doi: 10.1038/ng.487.

Singh, R.K., Soliman, A., Guaitoli, G., Stormer, E., von Zweydorf, F., Dal Maso, T., Oun, A., Van Rillaer, L., Schmidt, S.H., Chatterjee, D., David, J.A., Pardon, E., Schwartz, T.U., Knapp, S., Kennedy, E.J., Steyaert, J., Herberg, F.W., Kortholt, A., Gloeckner, C.J., and Versees, W. (2022). Nanobodies as allosteric modulators of Parkinson's disease-associated LRRK2. *Proceedings of the National Academy of Sciences of the United States of America 119* doi: 10.1073/pnas.2112712119.

Steger, M., Tonelli, F., Ito, G., Davies, P., Trost, M., Vetter, M., Wachter, S., Lorentzen, E., Duddy, G., Wilson, S., Baptista, M.A., Fiske, B.K., Fell, M.J., Morrow, J.A., Reith, A.D., Alessi, D.R., and Mann, M. (2016). Phosphoproteomics reveals that Parkinson's disease kinase LRRK2 regulates a subset of Rab GTPases. *Elife 5* doi: 10.7554/eLife.12813.

Stormer, E., Weng, J.H., Wu, J., Bertinetti, D., Kaila Sharma, P., Ma, W., Herberg, F.W., and Taylor, S. (2023). Capturing the domain crosstalk in full length LRRK2 and LRRK2RCKW. *The Biochemical journal* doi: 10.1042/BCJ20230126.

Taylor, S.S., Kaila-Sharma, P., Weng, J.H., Aoto, P., Schmidt, S.H., Knapp, S., Mathea, S., and Herberg, F.W. (2020). Kinase Domain Is a Dynamic Hub for Driving LRRK2 Allostery. *Frontiers in molecular neuroscience 13*, 538219 doi: 10.3389/fnmol.2020.538219.

Taymans, J.M., Fell, M., Greenamyre, T., Hirst, W.D., Mamais, A., Padmanabhan, S., Peter, I., Rideout, H., and Thaler, A. (2023). Perspective on the current state of the LRRK2 field. *NPJ Parkinsons Dis 9*, 104 doi: 10.1038/s41531-023-00544-7.

Taymans, J.M., Vancraenenbroeck, R., Ollikainen, P., Beilina, A., Lobbestael, E., De Maeyer, M., Baekelandt, V., and Cookson, M.R. (2011). LRRK2 kinase activity is dependent on LRRK2 GTP binding capacity but independent of LRRK2 GTP binding. *PloS one 6*, e23207 doi: 10.1371/journal.pone.0023207.

Traut, T.W. (1994). Physiological concentrations of purines and pyrimidines. *Mol Cell Biochem 140*, 1-22 doi: 10.1007/BF00928361.

Vetter, I.R., and Wittinghofer, A. (2001). The guanine nucleotide-binding switch in three dimensions. *Science 294*, 1299-1304 doi: 10.1126/science.1062023.

Wauters, L., Terheyden, S., Gilsbach, B.K., Leemans, M., Athanasopoulos, P.S., Guaitoli, G., Wittinghofer, A., Gloeckner, C.J., Versees, W., and Kortholt, A. (2018). Biochemical and kinetic properties of the complex Roco G-protein cycle. *Biol Chem 399*, 1447-1456 doi: 10.1515/hsz-2018-0227.

Webber, P.J., Smith, A.D., Sen, S., Renfrow, M.B., Mobley, J.A., and West, A.B. (2011). Autophosphorylation in the leucine-rich repeat kinase 2 (LRRK2) GTPase domain modifies kinase and GTP-binding activities. *Journal of molecular biology 412*, 94-110 doi: 10.1016/j.jmb.2011.07.033.

Wojewska, D.N., and Kortholt, A. (2021). LRRK2 Targeting Strategies as Potential Treatment of Parkinson's Disease. *Biomolecules 11* doi: 10.3390/biom11081101.

Wu, C.-X., Liao, J., Park, Y., Hoang, N.C., Engel, V.A., Wan, L., Oh, M., Sanishvili, R., Takagi, Y., Johnson, S.M., Wang, M., Federici, M., Nichols, R.J., Beilina, A., Reed, X., Cookson, M.R., and Hoang, Q.Q. (2019). A revised 1.6 Å structure of the GTPase domain of the Parkinson's disease-associated protein LRRK2 provides insights into mechanisms. Preprint available at *bioRxiv* doi: 10.1101/676627.

Wu, M., Yin, G., Zhao, X., Ji, C., Gu, S., Tang, R., Dong, H., Xie, Y., and Mao, Y. (2006). Human RAB24, interestingly and predominantly distributed in the nuclei of COS-7 cells, is colocalized with cyclophilin A and GABARAP. *Int J Mol Med 17*, 749-754 doi:

Zhu, H., Tonelli, F., Turk, M., Prescott, A., Alessi, D.R., and Sun, J. (2023). Rab29-dependent asymmetrical activation of leucine-rich repeat kinase 2. *Science 382*, 1404-1411 doi: 10.1126/science.adi9926.

Zimprich, A., Biskup, S., Leitner, P., Lichtner, P., Farrer, M., Lincoln, S., Kachergus, J., Hulihan, M., Uitti, R.J., Calne, D.B., Stoessl, A.J., Pfeiffer, R.F., Patenge, N., Carbajal, I.C., Vieregge, P., Asmus, F., Muller-Myhsok, B., Dickson, D.W., Meitinger, T., Strom, T.M., Wszolek, Z.K., and Gasser, T. (2004). Mutations in LRRK2 cause autosomal-dominant parkinsonism with pleomorphic pathology. *Neuron 44*, 601-607 doi: 10.1016/j.neuron.2004.11.005.

Figures and Tables

Tables:

LRRK2 variant	**K_M [µM]**	**k_{cat} [min^{-1}]**	**k_{cat}/K_M [min^{-1}/mM]**
wt	554 ± 62	0.36 ± 0.02	0.71 ± 0.08
wt + ATP	1036 ± 169	0.14 ± 0.01	0.13 ± 0.02
R1441G	272 ± 28	0.43 ± 0.02	1.57 ± 0.23
G2019S	867 ± 110	0.37 ± 0.03	0.42 ± 0.06
K1906M	181 ± 58	0.28 ± 0.03	1.52 ± 0.52
T1343A	265 ± 25	0.10 ± 0.01	0.38 ± 0.04
T1343A + ATP	328 ± 34	0.10 ± 0.01	0.30 ± 0.03

Table 1: HPLC-based full-length LRRK2 Michaelis-Menten kinetics

Figures:

Figure 1: Determination of kinetical parameters for LRRK2 GTP hydrolysis of PD variants by the Charcoal Assay. (A) Michaelis-Menten kinetics for pathogenic variant within the RocCOR module. (B) comparison of K_M values. (C) Comparison of k_{cat} values. (D) catalytic efficiency (k_{cat}/K_M). (E)-(G) Determination of k_{obs} values for full-length LRRK2 at 100µM (E) and 2000µM (F) GTP. (H) Domain structure of LRRK2 and the position of PD variants analyzed in this study.

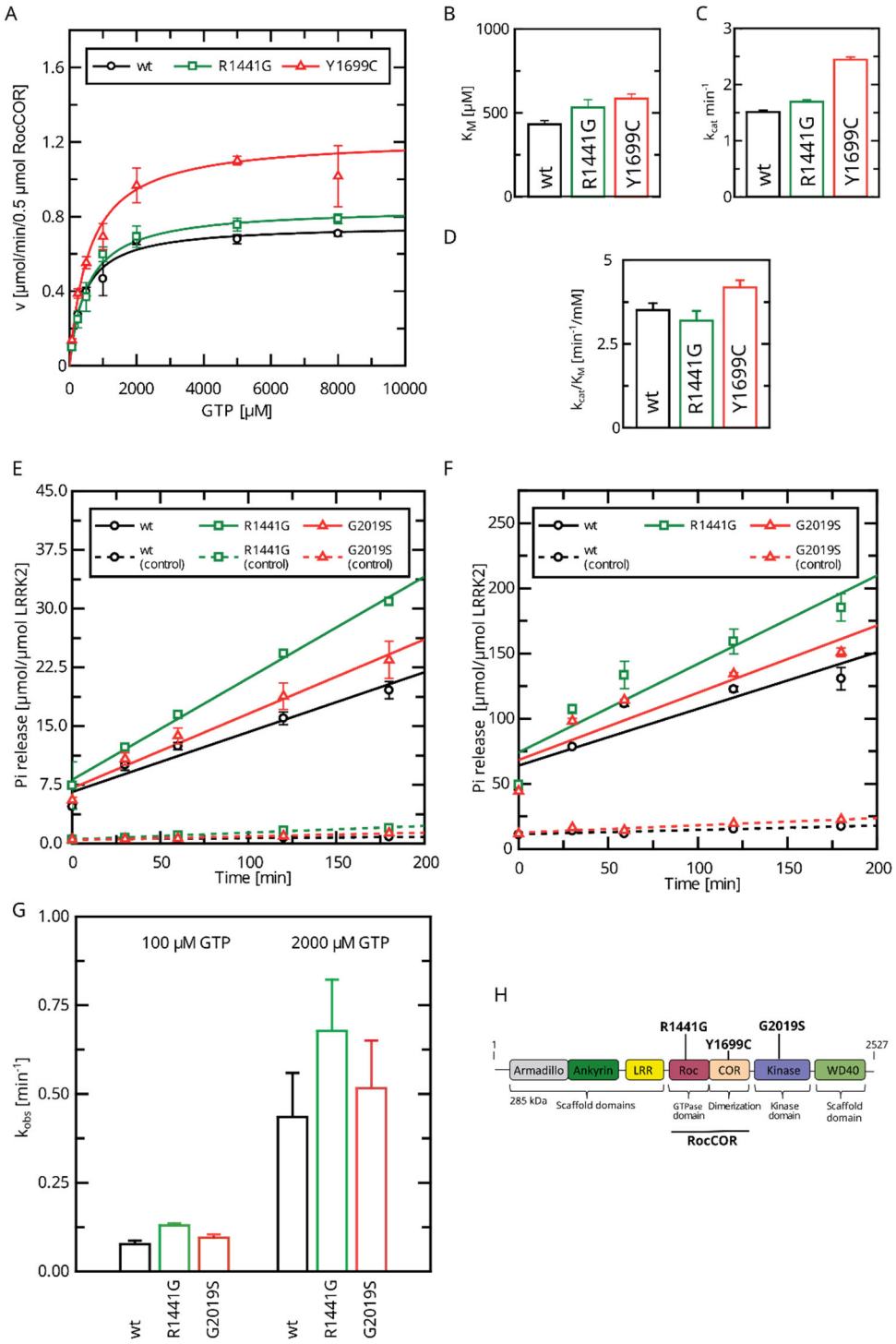

Figure 2: Comparison of PD mutants in the HPLC-based GTPase assay for the LRRK2 full-length protein. (A) Michaelis-Menten kinetics for the R1441G Roc-domain variant compared to LRRK2 wt. (B) Michaelis-Menten kinetics for the G2019S kinase-domain variant compared to LRRK2 wt. (C) Michaelis-Menten kinetics for a kinase-dead variant compared to LRRK2 wt.

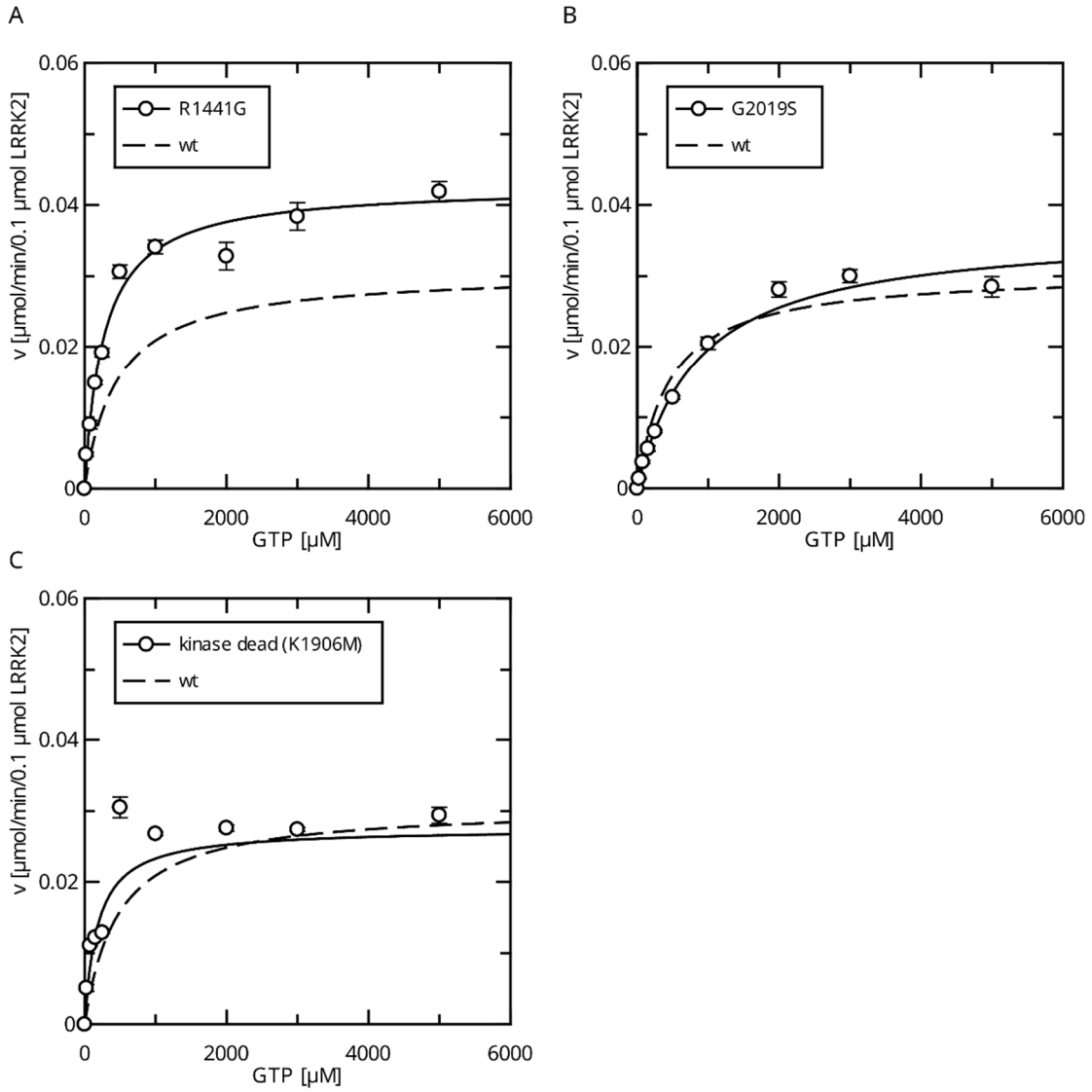

Figure 3: Identification of T1343 as relevant autophosphorylation site for a negative feedback loop. (A) Michaelis-Menten kinetics for LRRK2 wt +/- ATP, (B) Phospho-site screen: Position of the LRRK2 phosho-sites within the Roc domain which were included in the screen mapped on PDB:7LHW (Myasnikov et al., 2021). Individual domains are highlighted in color as follows: Armadillo (gray), Ankyrin (green), LRR (yellow), Roc (magenta), COR (wheat), Kinase (blue), WD40 (dark green). (C) Michaelis-Menten kinetics for T1343A LRRK2 +/- ATP.

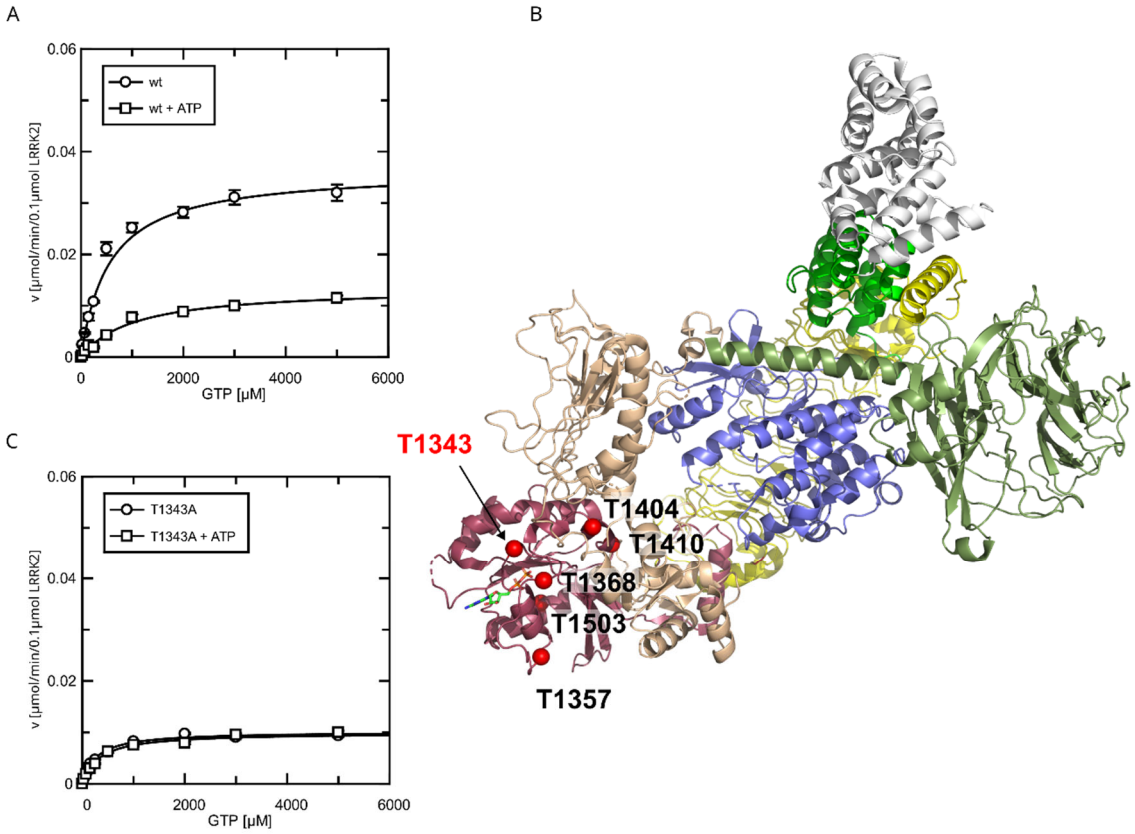

Figure 4: Overview of the kinetical parameters for fl. LRRK2 GTPase determined by the HPLC assay. (A) K_M values. (B) k_{cat} values and (C) catalytic efficiency (k_{cat}/K_M). Significant differences have been determined by an ANOVA followed by a post hoc test (p=0.05: *).

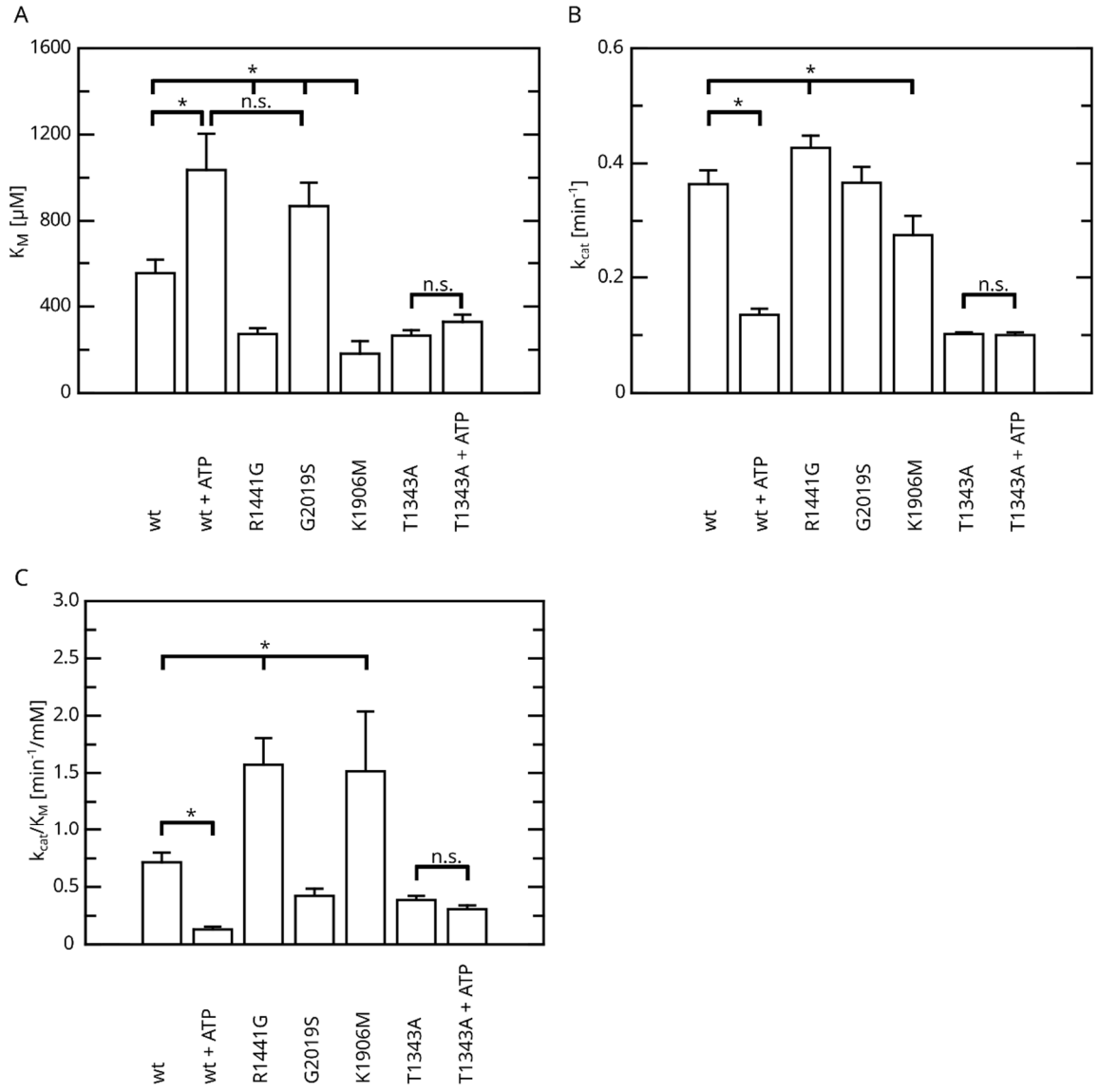

Figure 5: Effect of ATP incubation on the LRRK2 M/D equilibrium. (A) Mass photometry assays for LRRK2 wt and (B) T1343A LRRK2. Significance has been determined by a student's T-test (p=0.05: *; p=0.01: **).

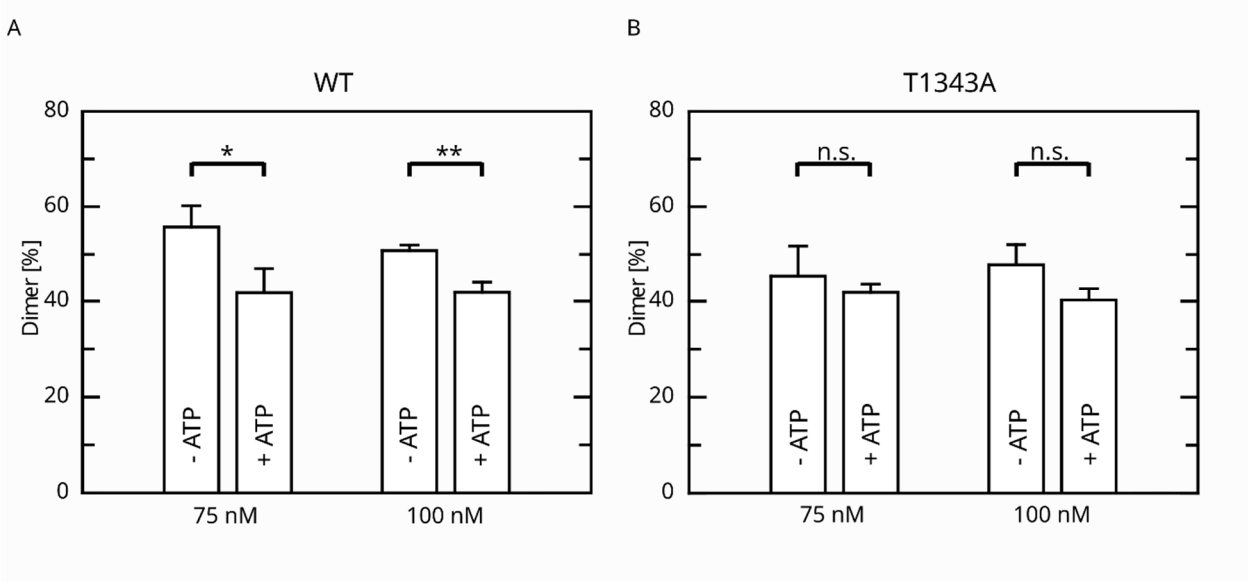

Figure 6: Effect of Roc T1343A on LRRK2 kinase activity and comparison to PD variants (A) *In vitro* LRRKtide HPLC-based kinase assay. (B) Western blot for LRRK2 pS935, total LRRK2, Rab10 pT73 and total Rab10. (C) Relative Rab phosphorylation levels. (D) Relative LRRK2 pS935 levels. Significant differences have been determined by an ANOVA followed by a post hoc test (p=0.05: *).

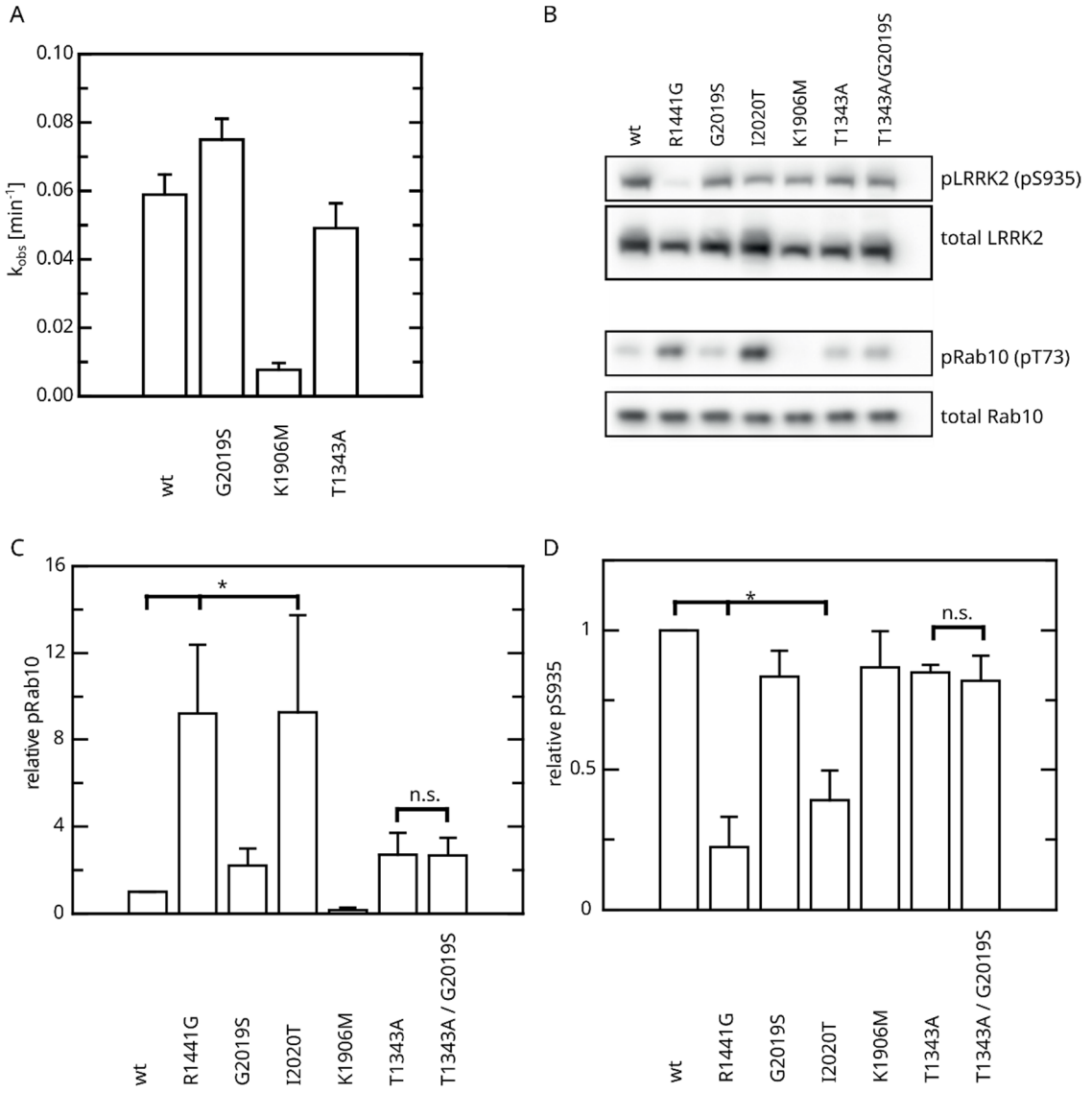

Supplemental Figures and Tables

Tables:

LRRK2 variant	**K_M [µM]**	**k_{cat} [min^{-1}]**	**k_{cat}/K_M [min^{-1}/mM]**
wt	431 ± 23	1.51 ± 0.03	3.51 ± 0.20
R1441G	545 ± 61	1.70 ± 0.06	3.19 ± 0.29
Y1699C	587 ± 28	2.44 ± 0.05	4.18 ± 0.21
T1343A	702 ± 69	2.64 ± 0.09	3.76 ± 0.40

Supplemental-Table 1: MBP-RocCOR Michaelis-Menten kinetics as measured by charcoal based GTPase assay.

LRRK2 variant	**k_{obs} [min^{-1}]** **100 µM GTP**	**k_{obs} [min^{-1}]** **2000 µM GTP**
wt	0.08 ± 0.01	0.44 ± 0.12
R1441G	0.13 ± 0.01	0.68 ± 0.14
G2019S	0.10 ± 0.01	0.52 ± 0.14

Supplemental-Table 2: GTPase activity (k_{obs}) as measured by charcoal based GTPase assay.

LRRK2 variant	**pRab10**	**pSer935**
wt	1.0 ± 0.0	1.0 ± 0.0
R1441G	8.0 ± 1.7	0.2 ± 0.1
G2019S	2.2 ± 0.8	0.9 ± 0.2
I2020T	7.3 ± 1.2	0.6 ± 0.3
K1906M	0.2 ± 0.1	1.0 ± 0.4
T1343A	2.1 ± 0.4	1.2 ± 0.6

T1343A/G2019S	2.5 ± 0.2	1.0 ± 0.4

Supplemental-Table 3: Cell-based phospho-Rab assays. Quantification of Western Blots

Figures:

Supplemental Figure 1: Michaelis-Menten kinetics for MLi-2 treated LRRK2 wt.

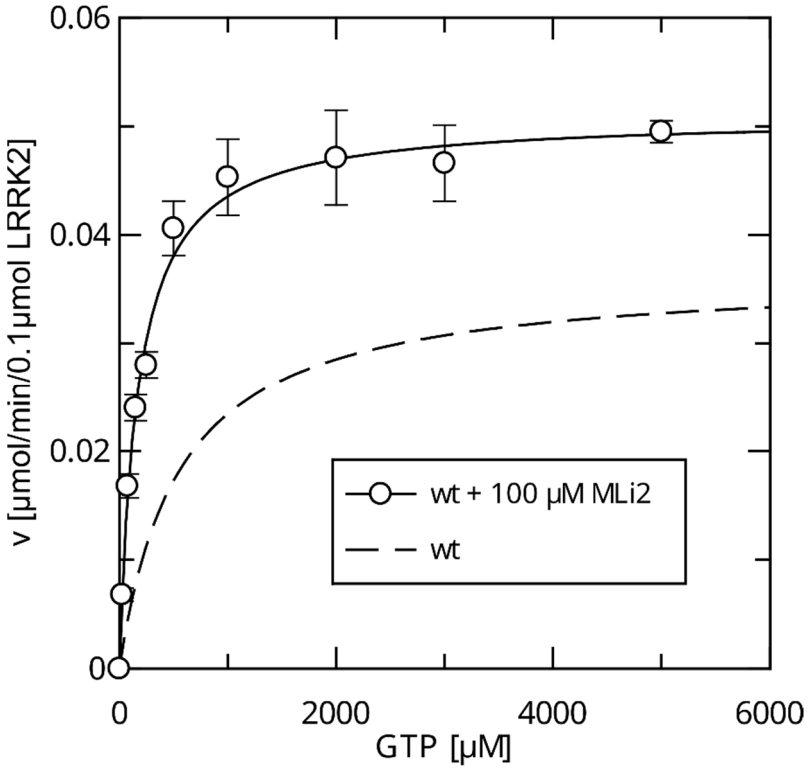

Supplemental Figure 2: Initial Phosphosite-screen (alanine screen). Michaelis-Menten parameters were determined in dependence of ATP pre-incubation. (A) K_M values. (B) k_{cat} values. The number of replicates is indicated.

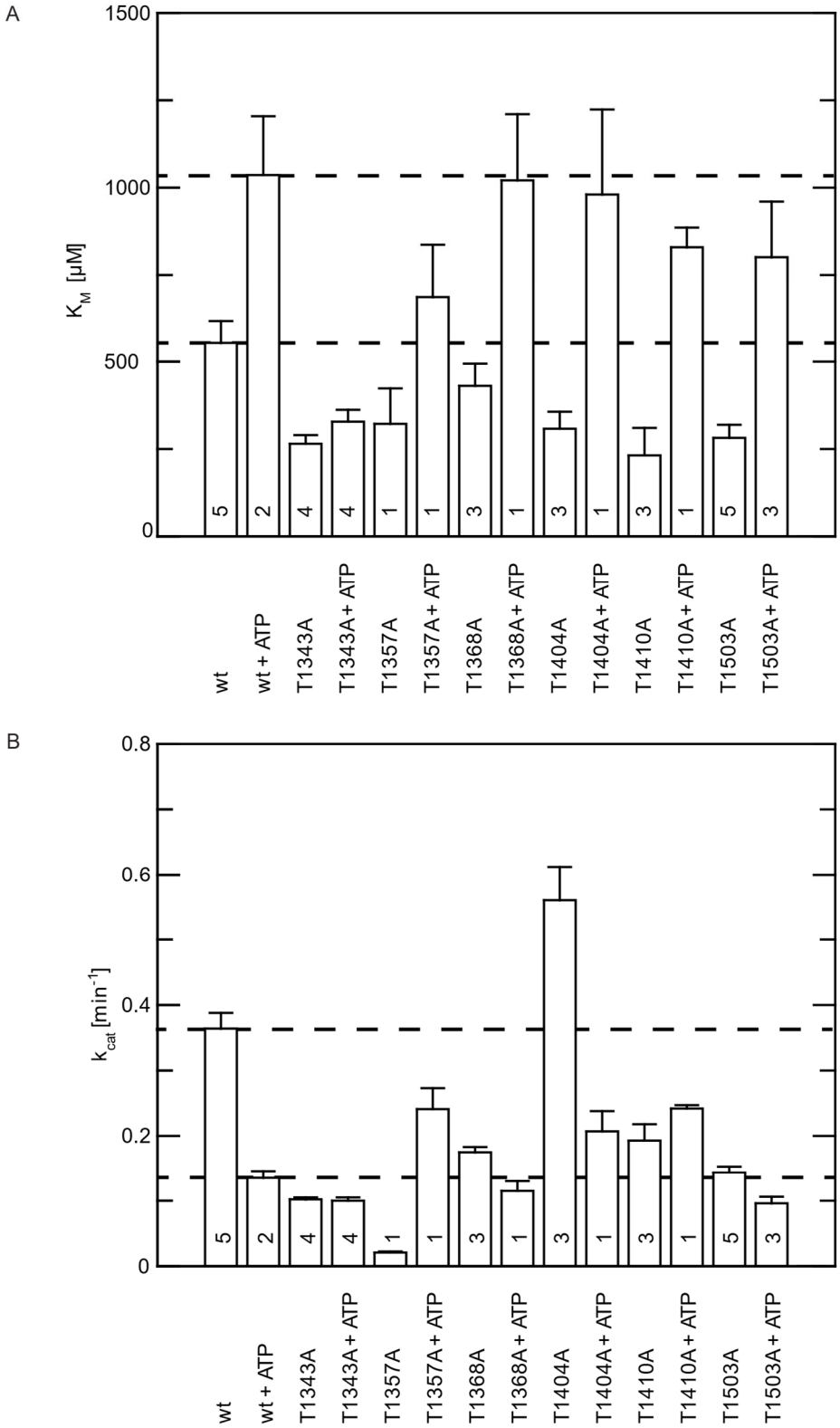

Supplemental Figure 3: Raw data for the *In vitro* LRRKtide HPLC Assay (determination of k_{obs} values). (A) LRRK2 G2019S, (B) LRRK2 wt, (C) LRRK2 T1343A, (D) kinase-dead (KD) LRRK2 K1906M.

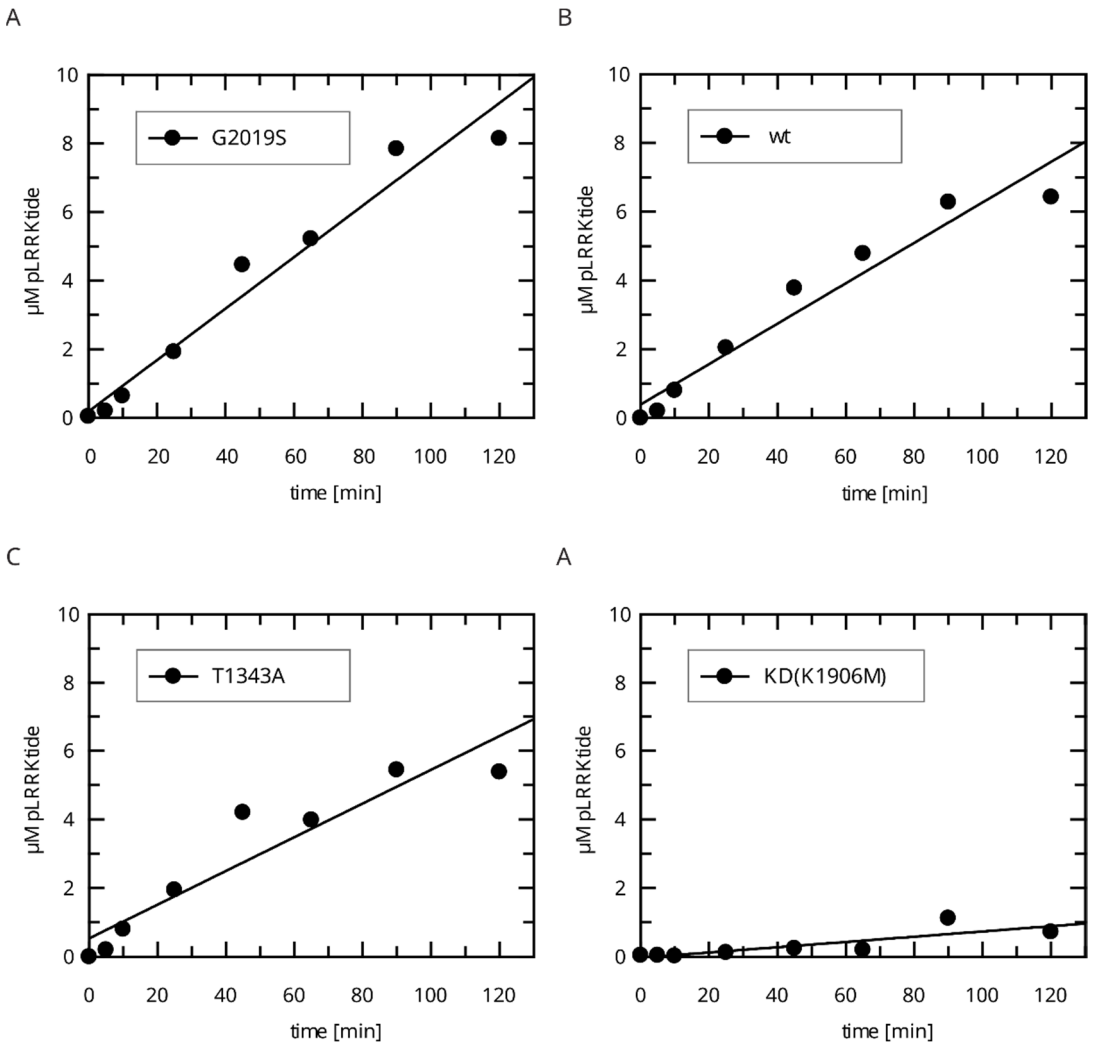

Supplemental Figure 4: Cell-based phosphor-Rab assays, blot raw images used for quantification. (A-C) biological replicates.

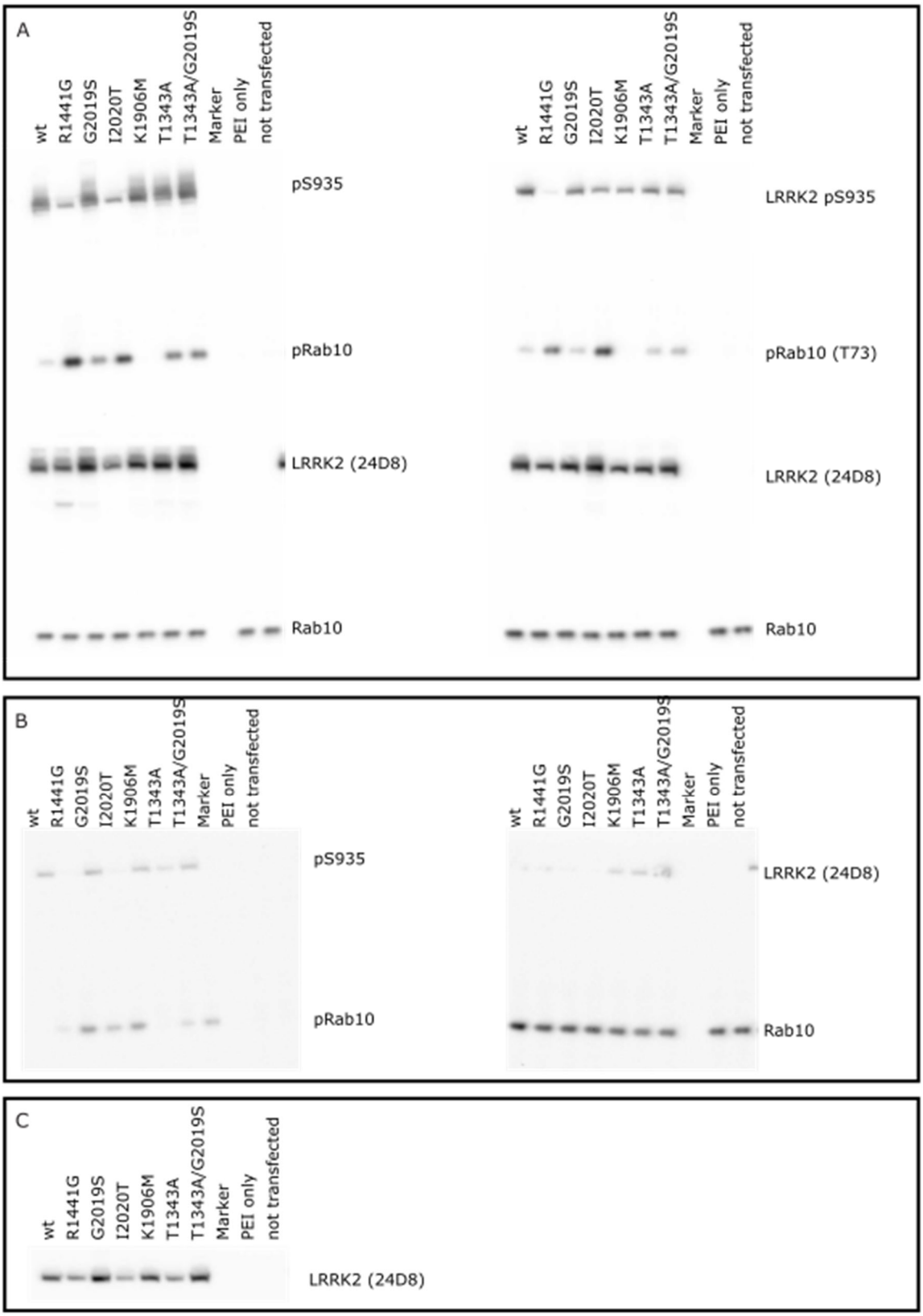

Detailed statistical analysis (Supplemental information for Figure 4):

(p values above 0.05 are shown in yellow)

K_M Anova (Std dev):

Between: 1962784.1180 d.f. 6 Variance: 327130.6863 F: 65.5951 p:0.0000

Within: 94755.3568 d.f. 19 Variance: 4987.1240

Total: 2057539.4748 d.f. 25

Tukey HSD Post-hoc Test:

wt vs wt + ATP: Diff=482.5208, 95%CI=288.4480 to 676.5936, p=0.0000

wt vs R1441G: Diff=-281.8767, 95%CI=-437.4811 to -126.2723, p=0.0002

wt vs G2019S: Diff=313.7215, 95%CI=158.1171 to 469.3259, p=0.0001

wt vs K1906M: Diff=-372.2505, 95%CI=-541.6511 to -202.8499, p=0.0000

wt vs T1343A: Diff=-288.5094, 95%CI=-444.1138 to -132.9050, p=0.0001

wt vs T1343A + ATP: Diff=-225.5213, 95%CI=-381.1257 to -69.9169, p=0.0022

wt + ATP vs R1441G: Diff=-764.3975, 95%CI=-965.2819 to -563.5131, p=0.0000

wt + ATP vs G2019S: Diff=-168.7993, 95%CI=-369.6837 to 32.0851, p=0.1364

wt + ATP vs K1906M: Diff=-854.7713, 95%CI=-1066.5220 to -643.0206, p=0.0000

wt + ATP vs T1343A: Diff=-771.0302, 95%CI=-971.9146 to -570.1458, p=0.0000

wt + ATP vs T1343A + ATP: Diff=-708.0421, 95%CI=-908.9265 to -507.1577, p=0.0000

R1441G vs G2019S: Diff=595.5982, 95%CI=431.5768 to 759.6196, p=0.0000

R1441G vs K1906M: Diff=-90.3738, 95%CI=-267.5372 to 86.7896, p=0.6389

R1441G vs T1343A: Diff=-6.6327, 95%CI=-170.6541 to 157.3887, p=1.0000

R1441G vs T1343A + ATP: Diff=56.3554, 95%CI=-107.6660 to 220.3768, p=0.9113

G2019S vs K1906M: Diff=-685.9720, 95%CI=-863.1354 to -508.8086, p=0.0000

G2019S vs T1343A: Diff=-602.2309, 95%CI=-766.2523 to -438.2095, p=0.0000

G2019S vs T1343A + ATP: Diff=-539.2428, 95%CI=-703.2642 to -375.2214, p=0.0000

K1906M vs T1343A: Diff=83.7411, 95%CI=-93.4223 to 260.9045, p=0.7117

K1906M vs T1343A + ATP: Diff=146.7292, 95%CI=-30.4342 to 323.8926, p=0.1464

T1343A vs T1343A + ATP: Diff=62.9881, 95%CI=-101.0333 to 227.0095, p=0.8607

k_{cat} Anova (Std. dev):

Between:	0.4441	d.f. 6	Variance: 0.0740	F: 165.1621	p:0.0000
Within:	0.0085	d.f. 19	Variance: 0.0004		
Total:	0.4526	d.f. 25			

Tukey HSD Post-hoc Test:

wt vs wt + ATP: Diff=-0.2290, 95%CI=-0.2872 to -0.1708, p=0.0000

wt vs R1441G: Diff=0.0630, 95%CI=0.0164 to 0.1096, p=0.0044

wt vs G2019S: Diff=0.0020, 95%CI=-0.0446 to 0.0486, p=1.0000

wt vs K1906M: Diff=-0.0890, 95%CI=-0.1398 to -0.0382, p=0.0003

wt vs T1343A: Diff=-0.2620, 95%CI=-0.3086 to -0.2154, p=0.0006

wt vs T1343A + ATP: Diff=-0.2640, 95%CI=-0.3106 to -0.2174, p=0.0008

wt + ATP vs R1441G: Diff=0.2920, 95%CI=0.2318 to 0.3522, p=0.0000

wt + ATP vs G2019S: Diff=0.2310, 95%CI=0.1708 to 0.2912, p=0.0000

wt + ATP vs K1906M: Diff=0.1400, 95%CI=0.0765 to 0.2035, p=0.0000

wt + ATP vs T1343A: Diff=-0.0330, 95%CI=-0.0932 to 0.0272, p=0.5635

wt + ATP vs T1343A + ATP: Diff=-0.0350, 95%CI=-0.0952 to 0.0252, p=0.4983

R1441G vs G2019S: Diff=-0.0610, 95%CI=-0.1102 to -0.0118, p=0.0096

R1441G vs K1906M: Diff=-0.1520, 95%CI=-0.2051 to -0.0989, p=0.0000

R1441G vs T1343A: Diff=-0.3250, 95%CI=-0.3742 to -0.2758, p=0.0321

R1441G vs T1343A + ATP: Diff=-0.3270, 95%CI=-0.3762 to -0.2778, p=0.0328

G2019S vs K1906M: Diff=-0.0910, 95%CI=-0.1441 to -0.0379, p=0.0004

G2019S vs T1343A: Diff=-0.2640, 95%CI=-0.3132 to -0.2148, p=0.0000

G2019S vs T1343A + ATP: Diff=-0.2660, 95%CI=-0.3152 to -0.2168, p=0.0000

K1906M vs T1343A: Diff=-0.1730, 95%CI=-0.2261 to -0.1199, p=0.0000

K1906M vs T1343A + ATP: Diff=-0.1750, 95%CI=-0.2281 to -0.1219, p=0.0000

T1343A vs T1343A + ATP: Diff=-0.0020, 95%CI=-0.0512 to 0.0472, p=1.0000

k_{cat}/K_M Anova (Std. dev):

Between:	7.0104	d.f. 6	Variance: 1.1684	F: 29.5277	p:0.0000
Within:	0.7518	d.f. 19	Variance: 0.0396		
Total:	7.7622	d.f. 25			

Tukey HSD Post-hoc Test:

wt vs wt + ATP: Diff=-0.5854, 95%CI=-1.1321 to -0.0387, p=0.0311

wt vs R1441G: Diff=0.8593, 95%CI=0.4210 to 1.2976, p=0.0001

wt vs G2019S: Diff=-0.2934, 95%CI=-0.7317 to 0.1449, p=0.3408

wt vs K1906M: Diff=0.8016, 95%CI=0.3244 to 1.2788, p=0.0004

wt vs T1343A: Diff=-0.3304, 95%CI=-0.7687 to 0.1079, p=0.2224

wt vs T1343A + ATP: Diff=-0.4104, 95%CI=-0.8487 to 0.0279, p=0.0755

wt + ATP vs R1441G: Diff=1.4447, 95%CI=0.8788 to 2.0106, p=0.0000

wt + ATP vs G2019S: Diff=0.2920, 95%CI=-0.2739 to 0.8579, p=0.6271

wt + ATP vs K1906M: Diff=1.3870, 95%CI=0.7905 to 1.9835, p=0.0000

wt + ATP vs T1343A: Diff=0.2550, 95%CI=-0.3109 to 0.8209, p=0.7526

wt + ATP vs T1343A + ATP: Diff=0.1750, 95%CI=-0.3909 to 0.7409, p=0.9440

R1441G vs G2019S: Diff=-1.1527, 95%CI=-1.6147 to -0.6907, p=0.0000

R1441G vs K1906M: Diff=-0.0577, 95%CI=-0.5567 to 0.4413, p=0.9997

R1441G vs T1343A: Diff=-1.1897, 95%CI=-1.6517 to -0.7277, p=0.0000

R1441G vs T1343A + ATP: Diff=-1.2697, 95%CI=-1.7317 to -0.8077, p=0.0000

G2019S vs K1906M: Diff=1.0950, 95%CI=0.5960 to 1.5940, p=0.0000

G2019S vs T1343A: Diff=-0.0370, 95%CI=-0.4990 to 0.4250, p=1.0000

G2019S vs T1343A + ATP: Diff=-0.1170, 95%CI=-0.5790 to 0.3450, p=0.9783

K1906M vs T1343A: Diff=-1.1320, 95%CI=-1.6310 to -0.6330, p=0.0000

K1906M vs T1343A + ATP: Diff=-1.2120, 95%CI=-1.7110 to -0.7130, p=0.0000

T1343A vs T1343A + ATP: Diff=-0.0800, 95%CI=-0.5420 to 0.3820, p=0.9970
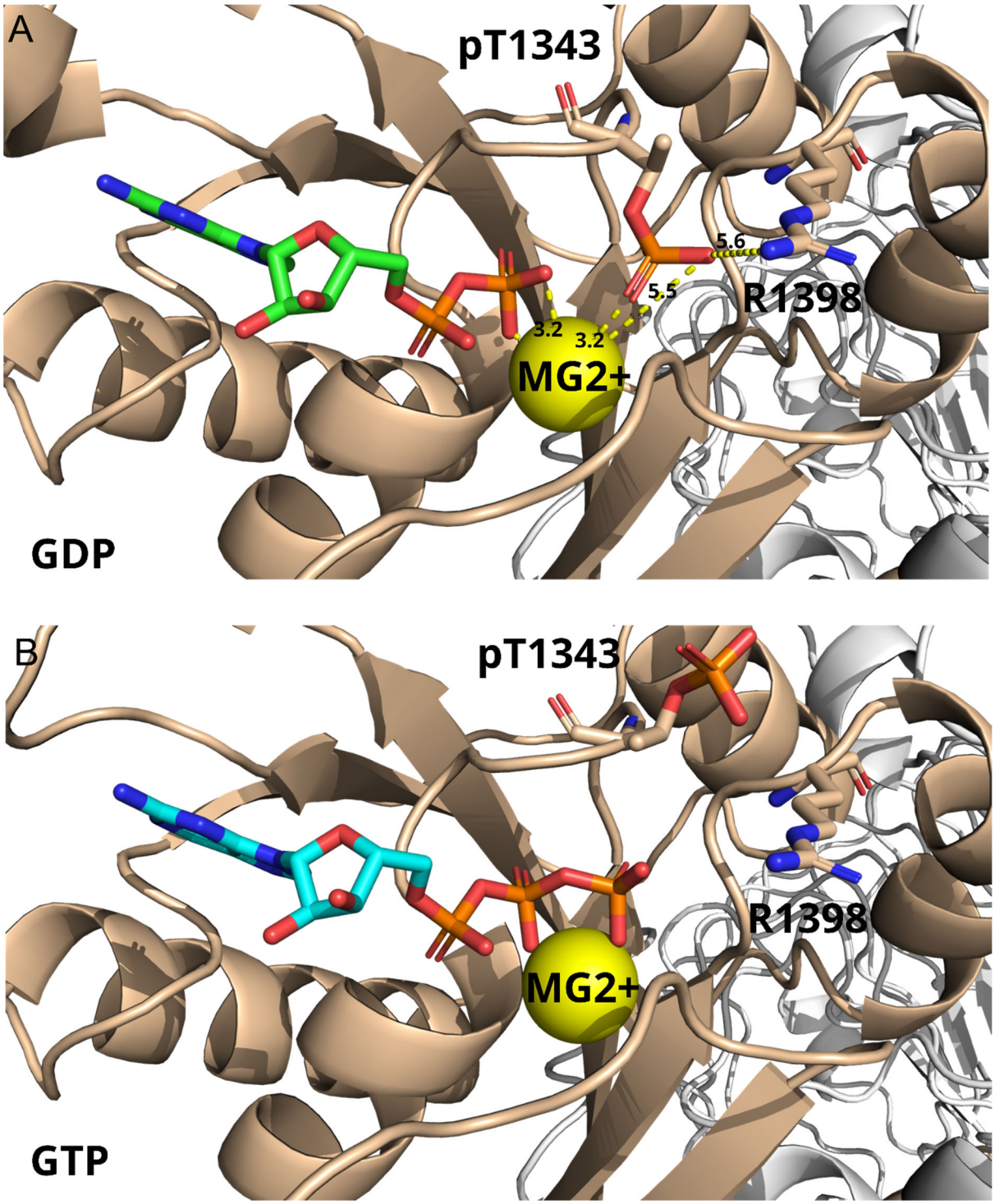
Supplemental Figure 5: AlphaFold 3 models of pT1343 LRRK2, in presence of either (A) GDP(Mg2+) or (B) GTP(Mg2+). Besides the residue pT1343, R1398 is highlighted in the structures. R1398 is in the homologous position to an invariant glutamine in the structure of small G proteins. The Q61 residue in Ras has been shown to be essential for the hydrolysis reaction as it coordinates the catalytic water molecule (Vetter and Wittinghofer, 2001). Distances shown in yellow report values in Ångström. Overall, the AF3 model represents the open (auto-inhibited state of LRRK2).